To appear in to the Astronomical Journal - Draft version December 7, 2010
Preprint typeset using LaTeX style emulateapj v. 11/10/09

LOW-MASS ECLIPSING BINARIES IN THE INITIAL *KEPLER* DATA RELEASE

J. L. Coughlin[1,5], M. López-Morales[2,3], T. E. Harrison[1], N. Ule[1], D. I. Hoffman[4]

To appear in to the Astronomical Journal - Draft version December 7, 2010

ABSTRACT

We identify 231 objects in the newly released Cycle 0 dataset from the *Kepler Mission* as double-eclipse, detached eclipsing binary systems with $T_{\rm eff} < 5500$ K and orbital periods shorter than $\sim$32 days. We model each light curve using the JKTEBOP code with a genetic algorithm to obtain precise values for each system. We identify 95 new systems with both components below 1.0 $M_{\odot}$ and eclipses of at least 0.1 magnitudes, suitable for ground-based follow-up. Of these, 14 have periods less than 1.0 day, 52 have periods between 1.0 and 10.0 days, and 29 have periods greater than 10.0 days. This new sample of main-sequence, low-mass, double-eclipse, detached eclipsing binary candidates more than doubles the number of previously known systems, and extends the sample into the completely heretofore unexplored P > 10.0 day period regime. We find preliminary evidence from these systems that the radii of low-mass stars in binary systems decrease with period. This supports the theory that binary spin-up is the primary cause of inflated radii in low-mass binary systems, although a full analysis of each system with radial-velocity and multi-color light curves is needed to fully explore this hypothesis. As well, we present 7 new transiting planet candidates that do not appear among the recently released list of 706 candidates by the *Kepler* team, nor in the *Kepler* False Positive Catalog, along with several other new and interesting systems. We also present novel techniques for the identification, period analysis, and modeling of eclipsing binaries.

Subject headings: stars: binaries: eclipsing — stars: binaries: general — stars: fundamental parameters — stars: late-type — stars: low-mass

1. INTRODUCTION

A double-lined, detached, eclipsing binary (DDEB) is a system that contains two non-interacting, eclipsing stars, in which the spectra of both components can be clearly seen, allowing for the radial-velocity (RV) of each component to be obtained. In these systems, the mass and radius of each star can be determined with errors usually less than 1-2%, thus making DDEBs currently the most accurate method of obtaining masses and radii of stars. Models of main-sequence stars with masses similar to or greater than the Sun have been tested over the years using DDEBs. Popper (1980) compiled available masses and radii of DDEB's with accuracies of ≤ 15%, up to that date, and found general agreement with stellar models, though stressed the need for more accurate observations and models. Andersen (1991) provided a compilation of all available DDEB systems up to that date, with accuracies ≤ 2%, and showed that the masses and radii of these stars were in general agreement with the current stellar evolution models, with any discrepancies attributable to abundance variations. Torres et al. (2010) recently performed a similar review with nearly double the sample of DDEBs. They were able to show the need to include non-classical effects such as diffusion and convection in stellar models, definitively demonstrate the existence of significant structural differences in magnetically active and fast-rotating stars, test theories of rotational synchronization and orbital circularization, and validate General Relativity via apsidal motion rates. However, while observations of DDEBs have enhanced our understanding of stellar structure and evolution for stars with $M \geq 1.0$ $M_{\odot}$, low-mass, main-sequence (LMMS) stars, ($M < 1.0$ $M_{\odot}$ and $T_{\rm eff} < 5800$ K), have not been tested to the same extent.

Although a couple systems with late G or early K type components had been studied prior to 2000, (c.f. Popper 1980; Andersen 1991; Torres et al. 2006; Clausen et al. 2009, and references therein), only three LMMS DDEBs with late K or M type components were known (Lacy 1977; Leung & Schneider 1978; Delfosse et al. 1999). This number had only increased to nine by the beginning of 2007 (cf. López-Morales 2007, Table 1). Despite the fact that the majority of main-sequence stars are low-mass, these stars are both intrinsically fainter, and physically smaller, than their more massive counterparts. Therefore, they have a lower eclipse probability and are harder to discover and study. As outlined by López-Morales (2007), analysis of these systems showed that the observed radii for these stars are consistently $\sim$10-20% larger than predicted by stellar models (Baraffe et al. 1998) for 0.3 $M_{\odot} \lesssim M \lesssim 0.8$ $M_{\odot}$. Fernandez et al. (2009) recently showed this was also likely the case for five M dwarfs in short-period eclipsing systems with an F type primary, though since the systems are only single-lined, the masses could not be determined directly. This discrepancy between the radii derived from models and from observations either reveals a flaw in the stellar models for this mass regime, or is

---

[1] Department of Astronomy, New Mexico State University, P.O. Box 30001, MSC 4500, Las Cruces, New Mexico 88003-8001
[2] Carnegie Institution of Washington, Department of Terrestrial Magnetism, 5241 Broad Branch Road NW, Washington, DC 20015, USA; Hubble Fellow
[3] Institut de Ciències de l'Espai (CSIC-IEEC), Campus UAB, Facultat de Ciències, Torre C5, parell, 2a pl, E-08193 Bellaterra, Barcelona, Spain
[4] California Institute of Technology, MC 249-17, 1200 East California Blvd, Pasadena, CA 91125
[5] NSF Graduate Research Fellow; jlcough@nmsu.edu

due to differences in metallicity, magnetic activity, or interpretation of the light curve data when star spots are present (Morales et al. 2008). As to this last point, Morales et al. (2010) recently noted that improperly taking polar spots into account in the light curve modeling process may possibly cause the derivation of stellar radii a few percent larger than the true values for some of these systems. Of all of these scenarios, enhanced magnetic activity has been proposed as the principal cause of inflated radii (Chabrier et al. 2007; López-Morales 2007; Morales et al. 2008).

If enhanced magnetic activity is the principal cause of the inflated radii, shorter-period binary systems, with the stellar rotation rate enhanced by the revolution of the system, would be expected to show greater activity and thus larger radii than longer-period systems (Chabrier et al. 2007). Binary systems with component masses of 0.5 $M_\odot$ are expected to synchronize, and therefore be spun-up, in less than 0.1 Gyr for periods less than 4 days, and in less than 1 Gyr for periods less than 8 days (Zahn 1977, 1994). Thus, the discovery of LMMS DDEBs with $P \gtrsim 10$ days, where the binary components should have natural rotation rates, is crucial to probing if enhanced rotation due to binarity is the underlying cause of this phenomenon. This theory might be supported by measurements of a couple isolated field M and K dwarf stars via very long baseline interferometry, which Demory et al. (2009) found to match stellar models. However, recently a much larger sample of nearly two dozen isolated M and K dwarf stars finds, for ∼80% of the sample, larger radii than the model predictions for $0.35 < M < 0.65\ M_\odot$ (Boyajian 2010), indicating that there are likely multiple causes of inflation at work, or a remaining flaw in the stellar models.

Though several more LMMS DDEB systems have been found since 2007, (Coughlin & Shaw 2007; Shaw & López-Morales 2007; Becker et al. 2008; Blake et al. 2008; Devor et al. 2008a,b; Shkolnik et al. 2008; Hoffman et al. 2008; Irwin et al. 2009; Dimitrov & Kjurkchieva 2010; Shkolnik et al. 2010), there are to-date only 7 well-studied systems with $1.0 < P < 3.0$ days (López-Morales 2007, and references therein) (Becker et al. 2008; Shkolnik et al. 2008), and only one has a larger period, at $P = 8.4$ days (Devor et al. 2008b). This is mostly due to the fact that ground-based photometric surveys, such as NSVS, TrES, and OGLE, are either cadence, precision, magnitude, or number limited, and thus not sensitive to long periods. The *Kepler Mission*, with 3 years of constant photometric monitoring of over 150,000 stars with $V \lesssim 17$, at 30-minute cadence and sub-millimagnitude precision, is the key to discovering a large number of long-period, LMMS DDEBs.

In this paper we present the results of our search through all the newly available *Kepler* Q0 and Q1 public data for LMMS DDEBs. Section 2 describes the data we use in this paper. Section 3 describes our binary identification technique, and Section 4 describes how we model the light curves. Our selection and list of new LMMS DDEBs is presented in Section 5, and we present new transiting planet candidates in Section 6. In Section 7 we compare the new LMMS DDEBs with theoretical models, and conclude with a summary of our results in section 8. Once accurate mass and radius values exist for a large range of both mass and period, our understanding of these objects should substantially improve, and we will be one step closer to extending to the lower-mass regime the advanced study of stellar structure and evolution that sun-like and high-mass stars have been a subject of for some time.

2. OBSERVATIONAL DATA

The data used in our analysis consists of the 201,631 light curves made public by the *Kepler Mission*[6] as of June 15, 2010 from *Kepler* Q0 and Q1 observations. All light curves can be accessed through the Multi-mission Archive at STScI (MAST)[7]. The data consist of 51,366 light curves from *Kepler* Q0, (observed from 2009-05-02 00:54:56 to 2009-05-11 17:51:31 UT), and 150,265 light curves from *Kepler* Q1, (observed from 2009-05-13 00:15:49 to 2009-06-15 11:32:57 UT), each at 29.43 minute cadence. Individual light curves for Q0 contain ∼470 data points, and for Q1 contain ∼1,600 data points. Targets range in *Kepler* magnitude from 17.0 at the faintest, to 5.0 at the brightest.

The *Kepler* team has performed pixel level calibrations, (including bias, dark current, flat-field, gain, and non-linearity corrections), identified and cleaned cosmic-ray events, estimated and removed background signal, and then extracted time-series photometry using an optimum photometric aperture. They have also removed systematic trends due to spacecraft pointing, temperature fluctuations, and other sources of systematic error, and corrected for excess flux in the optimal photometric aperture due to crowding (Van Cleve 2010). It is this final, "corrected" photometry that we have downloaded for use in our analysis.

3. ECLIPSING BINARY IDENTIFICATION

Prša et al. (2010) have recently released an initial catalog of eclipsing binary stars they find in the *Kepler* field from the same Q0 and Q1 data we use in this paper. They first identified EB candidates via *Kepler's* Transit Planet Search (TPS) algorithm, eliminating those targets already identified as exoplanet candidates. To determine the ephemeris of each candidate, they used Lomb-Scargle, Analysis of Variance, and Box-fitting Least Squares periodogram techniques, combined with manual inspection and modification. They then culled, through manual inspection, non-EB candidates, such as pulsating and heavily spotted stars, as well as duplicates due to contamination from nearby stars, and arrive at their final list of 1,832 binaries, which are manually classified as detached, semi-detached, over-contact, ellipsoidal, or unknown. Next, they estimate the principal parameters of each system, (temperature ratio, sum of the fractional radii, $e \cdot \cos(\omega)$, $e \cdot \sin(\omega)$, and $\sin(i)$ for detached systems), via a neural network technique called Eclipsing Binaries via Artificial Intelligence ("EBAI" Prša et al. 2008). For our search, which focuses on the detection of LMMS DDEBs, we have devised our own DDEB identification technique, which we apply to the Q1 data. We do not use the Q0 data in this part of the analysis to avoid discrepant systematics between the two quarters, which complicate the analysis.

---

[6] http://kepler.nasa.gov/

[7] http://archive.stsci.edu/kepler/

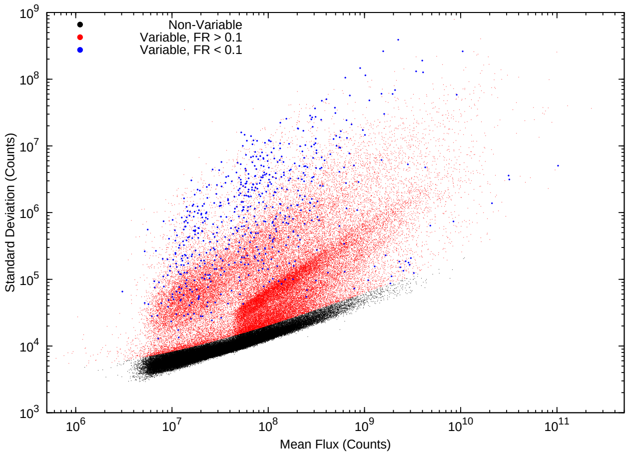

Figure 1. Plot of standard deviation versus mean flux for the 150,265 stars in Q1. Black dots represent stars that vary by less than 1-sigma from a best-fit power-law to the data, and thus we classify them as non-variables. Red dots represent variables with a flux ratio greater than 0.1. Blue dots represent variables with a flux ratio less than 0.1, and thus are good candidates to be eclipsing binaries.

Our search consisted of two steps. The first was to identify variable stars, and to do so, we placed a light curve standard deviation limit above which the objects are classified as variables. We first subtracted an error-weighted, linear fit of flux versus time from all data, to remove any remaining linear systematic trends, and then plotted the standard deviation of each light curve versus its average flux and fit a power law. These data are shown in Figure 1, where the black dots correspond to light curves which deviate by less than 1σ from the standard deviation versus average flux fit, and we thus classify as non-variable. The colored dots indicate the variable candidates that deviate by more than 1σ. Next, we used the flux ratio (FR) measurement criterion, which we adapted from the magnitude ratio given in Kinemuchi et al. (2006), and is defined as

$$\mathrm{FR} = \frac{\text{maximum flux - median flux}}{\text{maximum flux - minimum flux}} \tag{1}$$

as a measure of whether or not the variable spends most of its time above (low FR value) or below (high FR value) the median flux value. Perfectly sinusoidal variables have $\mathrm{FR} = 0.50$, pulsating variables, such as RR Lyrae's, have $\mathrm{FR} > 0.5$, and eclipsing binaries have $\mathrm{FR} < 0.5$. As we are principally interested in finding well detached systems with relatively deep, narrow eclipses, which thus have low FR values, we make a further cut of the systems and only examine those variables with $\mathrm{FR} < 0.1$, shown by blue dots in Figure 1.

The second step of the analysis was to determine the orbital period of each candidate. This was done using two independent techniques that are both well-suited for detached eclipsing binary systems. The first is Phase Dispersion Minimization (PDM) (Stellingwerf 1978), which attempts to find the period that best minimizes the variance in multiple phase bins of the folded light curve. This technique is not sensitive to the shape of the light curve, and thus is ideal for non-sinusoidal variables such as detached eclipsing binaries. The downside of this technique is that if strong periodic features exist in the light curve, which do not correspond to the period of eclipses, such as rapidly varying spots, stellar pulsations, or leftover systematics, they can weaken the signal of the eclipse period. We use the latest implementation given by Stellingwerf (2006), and determine the best three periods via this technique to ensure that the true period is found, and not just an integer multiple, or fraction, thereof.

The second technique we use is one we invented specifically for detached eclipsing binaries, and call Eclipse Phase Dispersion Minimization (EPDM). The idea behind EPDM is that we want to automatically identify and align the primary eclipses in an eclipsing binary, thus finding the period of the system. To accomplish this, EPDM finds the period that best minimizes the dispersion of the actual phase values of the faintest N points in a light curve, i.e. the very bottom of the eclipses. Since EPDM only selects the N faintest points in a light curve, it is not affected by systematics or periodic features that do not correspond to the period of eclipses, assuming the systematics do not extend below the depth of the eclipses. The technique works for all binary systems with equal or unequal eclipse depths, and transiting planets, both with either zero or non-zero eccentricity. Computationally, EPDM is significantly faster than traditional PDM techniques. For a detailed and illustrative explanation of this new technique, please see Appendix A. We use EPDM to find the three best fit periods for each system as well, for the same reasons as we did with PDM.

We identify 577 EB candidates in the Q1 data. Of these, 486 are listed by Prša et al. (2010) as detached eclipsing binaries, and 20 are identified as semi-detached eclipsing binaries. The 71 remaining candidates were manually inspected by examining both the raw and phased light curves at the 6 best periods found via PDM and EPDM. Of these 71 remaining candidates, 48 turned out to be false positives with significantly large, sharp systematic features, and one is an apparent red giant, (Kepler 010614012, $\mathrm{T_{eff}} = 4859\mathrm{K}$, logg = 3.086, [M/H] = -0.641, $\mathrm{R}_\star = 5.708\ \mathrm{R}_\odot$), with an unusual, asymmetrical, eclipse-like feature that lasts for ∼3 days with a depth of 1.2%, shown in Figure 2. This does not appear to be a systematic feature due to its very flat out of eclipse baseline, contiguous nature, long duration, and the actual time at which the feature occurs, compared to the majority of other objects with strong systematics. The remaining 22 targets are: 2 transiting exoplanet candidates contained in the recently released list of 306 candidates by Borucki & the Kepler Team (2010), 3 already published transiting planets, (Kepler-5b, Kepler-6b, and TrES-2b), 7 shallow eclipsing systems with primary eclipse depths ranging from 1.4% to 5.7%, visible secondary eclipses ranging from 0.05% to 4.6%, and periods ranging from 4.7 to 45.3 days, the already published transiting hot compact object Kepler 008823868 (Rowe et al. 2010), a 6.4 day eclipsing binary with $\mathrm{T_{eff}} = 5893\mathrm{K}$ and eclipse depths of 38.4% and 12.2% (Kepler 006182849), and 8 transiting exoplanet candidates with transit depths ranging from 0.75% to 4.9%, and periods ranging from 2.5 to 24.7 days. For the 7 new extremely shallow eclipsing systems, we list their *Kepler* ID numbers, periods, effective temperatures, surface gravities, and primary and secondary eclipse depths in Table 1, and note they could be of interest for follow-up due to the potential to contain brown dwarf or extremely low-mass secondaries, or even anomalously hot exoplanet compan-

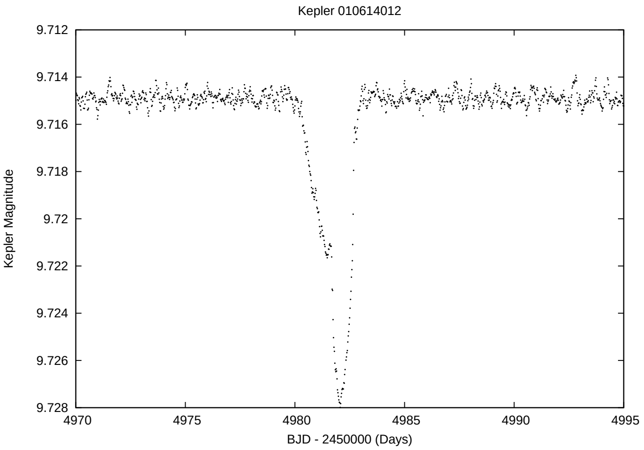

Figure 2. Kepler 010614012. An apparent red giant, (T_{eff} = 4859K, logg = 3.086, [M/H] = -0.641, $R_\star$ = 5.708 $R_\odot$), with a very unusual, shallow, eclipse-like feature.

ions. Of the 8 transiting candidates, only one is listed in the *Kepler* false positive catalog[8], Kepler 011974540. None of them are in the list of the 306 released candidates by Borucki & the Kepler Team (2010), nor are among the 400 planetary candidates currently reserved for follow-up observations (Borucki & the Kepler Team 2010). These will be further discussed in Section 6.

4. LIGHT CURVE MODELING

Since the system parameters determined by Prša et al. (2010) are only estimates and do not incorporate spots, and since we seek to obtain as accurate physical parameters as possible, we modeled each system using a robust global minimization scheme with a commonly used, physically detailed eclipsing binary modeling code. We took all 314 detached eclipsing binaries with $T_{\mathrm{eff}} < 5500$K and that are publicly available, (5 systems are still proprietary), identified from both our search and the Prša et al. (2010) catalog, combined Q0 and Q1 data if available, and via manual inspection classified systems as double-eclipse (i.e. contained two visible eclipses), single-eclipse (i.e. only contained one eclipse), or as spurious results that were not recognizable as eclipsing systems. (Given the errors in the KIC temperature determination, and to ensure the primary is below 1.0 $M_\odot$, we used 5500K as our cutoff, instead of 5800K. As well, the definition of a "double-lined" system is one in which the lines of both components are visible in an observed spectrum. Although in general if two eclipses are clearly visible in the photometric light curve, it is likely to be "double-lined", this cannot be determined without an actual spectrum. Thus, we use the term "double-eclipse" throughout the paper, with the assumption that when observed spectroscopically, the majority of these systems will be observed as "double-lined".)

We then used the JKTEBOP eclipsing binary modeling program (Southworth et al. 2004a,b) to model every double-eclipse eclipsing binary system, of which there were 231, solving for the period, time of primary minimum, inclination, mass ratio, e·cos(ω), e·sin(ω), surface brightness ratio, sum of the fractional radii, ratio of the radii, and out of eclipse flux. In addition, we also solved for the amplitude and time of minimum of a sinusoidal term imposed on the luminosity of the primary component, with the period fixed to that of the binary, in order to account for spots. Note that in the JKTEBOP model the mass ratio is only used to determine the amount of tidal deformation of the stars from a pure sphere. Thus, it has no effect on the light curve of long-period systems, which due to their large separations are almost perfectly spherical, but must be included to properly model very short-period systems, where the tidal deformation can have a significant impact on the light curve. We used the quadratic limb darkening law, which works well for late-type stars (e.g. Manduca et al. 1977; Wade & Rucinski 1985; Claret & Gimenez 1990), with coefficients set to those found by Sing (2010) for the *Kepler* bandpass via interpolation given the systems' effective temperatures, surface gravities, and metallicities as listed in the Kepler Input Catalog (KIC)[9]. We also fixed the gravity darkening exponent based on the effective temperature as prescribed by Claret (2000). As any contaminating flux from nearby stars in the photometric aperture has already been compensated for in the *Kepler* pipeline (Van Cleve 2010), we set the amount of third light to 0.0. Note that third light might still exist in some systems if there is a background star or tertiary component that is unidentifiable from ground-based surveys, (i.e. less than $\sim 1''$ separation), but since third light is usually unconstrained in a single-color light curve, we do not let it vary. If third light existed in a system and was not accounted for, the solution would result in an inclination determination lower than the true value, and therefore an over-estimation of the stellar radius. However, this should only occur in a minority of systems. For a couple binaries in our list, the light curves absolutely could not be modeled without the inclusion of third light, (i.e. very sharp eclipses with depths of less than 0.01 mag). For these cases only, we let the third light vary, and thus be a non-zero parameter. Additionally, if the effect of spots in a light curve deviates significantly from the adopted sinusoidal shape, it could affect the derived luminosity ratio to a minor extent, but it should not affect the sum of the radii.

In order to model such a large number of systems over

Table 1
Period, Effective Temperature, Surface Gravity, and Eclipse Depth Estimates for the 7 New Extremely Shallow Eclipsing Systems

Kepler ID	Period (Days)	T_{eff} (K)	logg	Pri. (%)	Sec. (%)
003098197	38.3840[3]	5675	4.814	4.9	4.60
004178389[1]	45.2600[3]	5645	4.670	3.4	2.80
009016295[2]	19.9858	5819	4.582	4.1	0.17
009071386[1]	4.68513	6324	4.267	1.4	0.05
009838975[1]	18.7000	5018	4.802	5.7	0.21
012017140[2]	22.8624	6026	4.500	4.7	0.11
012504988[1]	5.09473	5985	4.464	2.9	0.06

[1] System is listed in the *Kepler* False Positive Catalog as likely to be an EB.
[2] System has non-zero eccentricity.
[3] Period derived assuming zero eccentricity.

---

[8] http://archive.stsci.edu/kepler/false_positives.html

[9] http://archive.stsci.edu/kepler/kepler_fov/search.php

such a large solution space, and to ensure we have found the best global solution, we adapted the JKTEBOP code to use a modified version of the asexual genetic algorithm (AGA) described by Cantó et al. (2009), coupled with its standard Levenberg-Marquardt minimization algorithm. Genetic algorithms (GA) are an extremely efficient method of fitting computationally intensive, multi-parameter models over a large and potentially discontinuous parameter space, and thus ideal for this work. For the details of how genetic algorithms work, and the specific changes we made to the Cantó et al. (2009) AGA, please see Appendix B.

We found that our modified AGA does an excellent job of solving well-behaved light curves, simultaneously varying all 12 aforementioned parameters over the entire range of possible solutions. For some of the systems however, strong systematics and/or variable star spots introduced a significant amount of noise, especially in systems with shallow eclipses, for which it was more difficult to arrive at a robust solution. For these systems we had to manually correct the systematics, often by either eliminating the Q0 or Q1 data, equalizing the base flux levels of Q0 and Q1 data, or subtracting out a quasi-sinusoidal variation in the base flux level due to remaining *Kepler* systematics. When possible we attempted to minimize the amount of manual interference. Hopefully this will become much less of a problem with subsequent data releases. We then re-ran the AGA using a larger initial population until a good solution was found. Every light curve in the end was visually inspected to be a good fit compared to the scatter of the data points, and the obtained parameters were confirmed to be reasonable when visually inspecting the light curves.

5. NEW LOW-MASS BINARY CANDIDATES

In order to identify the main-sequence stars from our list of 231 candidates, and determine the best candidates for follow-up, we employ the following technique to estimate the temperature, mass, and radius of each star using the sum of the fractional radii, r_{sum}, and period, P, obtained from our JKTEBOP models, the luminosity ratio, L_r, (which is derived from the surface brightness ratio, J, and radii ratio, k, obtained from the models), and the effective temperature of the system, T_{eff}, obtained from the KIC, with an estimated error of ±200 K.

The value for T_{eff} given in the KIC was determined via interpolation of standard color magnitude relations as determined by ground-based, multi-wavelength photometry (Van Cleve 2010). Although in principle one might be able to deconvolve two separate spectral energy distributions from this photometry, in reality given the level of photometric error in the KIC and uncertainty at which binary phase the photometry was obtained, this is untenable. Instead, we assume the stars radiate as blackbodies, and that each star contributes to the determined T_{eff} in proportion to its luminosity. Thus, following our assumption, we obtain the following relation,

$$T_{\text{eff}} = \frac{L_1 T_1 + L_2 T_2}{L_1 + L_2} \tag{2}$$

where L_1, L_2, T_1 and T_2 are the luminosities and effective temperatures of star 1 and 2 respectively. Still assuming the stars radiate as blackbodies, the luminosity of each star is proportional to its radius squared and temperature to the fourth power, with the temperature proportional to is surface brightness to the one-fourth power. Thus, we find that the luminosity ratio can be expressed as,

$$\begin{aligned} L_r = & \frac{L_1}{L_2} = \frac{r_1^2 T_1^4}{r_2^2 T_2^4} = k^2 T_r^4 = k^2 \left[\left(\frac{SB_1}{SB_2} \right)^{1/4} \right]^4 \\ = & k^2 \left(J^{\frac{1}{4}} \right)^4 = k^2 J \end{aligned} \tag{3}$$

where SB_1 and SB_2 are the surface brightnesses of star 1 and star 2 respectively, and r_1 and r_2 are the fractional radii of star 1 and 2 respectively, defined as R_1/a and R_2/a, where R_1 and R_2 are the physical radius of each star, and a is the semi-major axis of, or separation between, the components. Combining equations 2 and 3 yields the expression,

$$T_{\text{eff}} = \frac{L_r T_1 + T_2}{L_r + 1} \tag{4}$$

which has two known parameters, T_{eff} and L_r, and two unknown parameters, T_1 and T_2. To place a further constraint upon the values of T_1 and T_2, we make the assumption that both stars in the binary are on the main-sequence, and employ the mass, temperature, radius, and average of the V-band and R-band luminosity relations given in Baraffe et al. (1998) for $0.075 \leq \text{M} \leq 1.0\ \text{M}_\odot$ and in Chabrier et al. (2000) for $\text{M} < 0.075\ \text{M}_\odot$, both assuming an age of 5.0 Gyr and [M/H] = 0.0. (We average the V and R-band luminosities to obtain a very close approximation to the *Kepler* bandpass.) From these models, for a given value of T_1, there is only one value of T_2 which will reproduce the observed value of L_r. Thus, there only exists one set of unique values for T_1 and T_2 that reproduces both the observed T_{eff} and L_r values for the system.

For each T_1 and T_2 then, we obtain the absolute masses and radii, (M_1, M_2, R_1, and R_2), via interpolation from the Baraffe et al. (1998) and Chabrier et al. (2000) models. Then, utilizing Kepler's 3^{rd} law, given the total mass of the system, we calculate the semi-major axis, a, via

$$a = (GM_{tot})^{\frac{1}{3}} (\frac{P}{2\pi})^{\frac{2}{3}} \tag{5}$$

where M_{tot} is the total mass of the system, $\text{M}_1 + \text{M}_2$, and G is the gravitational constant. We then multiply each radius determined above by a constant so that the sum of the fractional radii derived from the JKTEBOP model, r_{sum}, is equal to $(R_1 + R_2)/a$, the sum of the fractional radii when using the physical values of M_1, M_2, R_1, R_2, and P. This technique is robust because while individual parameters such as i, J, and k can suffer from degeneracies, especially in systems with shallow eclipses, the values of r_{sum} and $L_r = k^2 J$, which we rely on, are firmly set by the width of the eclipses and the difference in their eclipse depths, respectively.

For clarity, we now illustrate the individual steps of this procedure using the example of an actual system, Kepler 002437452. This system was found to have $T_{\rm eff}$ = 5398 K and L_r = 3.90 from the KIC and the JKTEBOP modeling respectively. Now, assuming the stars are main-sequence, one could choose values of T_1 = 4000 K and T_2 = 3620 K, and looking up their luminosities from the Baraffe et al. (1998) models, find that the luminosity ratio between two main-sequence stars with temperatures of 4000 K and a 3620 K is 3.90. In this case, the luminosity ratio criterion would be satisfied, but $T_{\rm eff}$ would would be ∼3922 K, nowhere near the measured value of 5398 K. Similarly, one could choose values of T_1 = 5400 and T_2 = 5393, and this would yield $T_{\rm eff}$ = 5398 K, but L_r would be 1.01, nowhere near the needed value of 3.90. The unique solution that satisfies both the effective temperature and luminosity ratio constraints is that T_1 = 5591 and T_2 = 4647, which yields both $T_{\rm eff}$ = 5398 and L_r = 3.90. Now, given these temperatures, interpolating from the Baraffe et al. (1998) models yields values of $M_1 = 0.963\ M_\odot$, $R_1 = 0.966\ R_\odot$, $M_2 = 0.792\ M_\odot$, and $R_2 = 0.783\ R_\odot$. Taking the masses, and the period of the system of 14.47184 days, and utilizing Eq. 5, we find that the semi-major axis, a, would be 30.1 $R_\odot$. Dividing the sum of the estimated physical radii by the semi-major axis just calculated, we find a value of 0.058 for the sum of fractional radii. Now, from the JKTEBOP model, this system was measured to have a sum of the fractional radii of 0.084, and so it appears that the current values for the radii are underestimated. Thus, we multiply the radii by a factor of 0.084/0.058 = 1.45, to obtain our final radii values of $R_1 = 1.40\ R_\odot$ and $R_2 = 1.13\ R_\odot$, with, as above, $M_1 = 0.96\ M_\odot$, T_1 = 5591 K, $M_2 = 0.79\ M_\odot$, and T_2 = 4647 K.

Kipping (2010) has recently examined the effects of the long, (∼30 minute), integration time of long-cadence *Kepler* observations on transit light curves, and found that it can significantly alter the morphological shape of a transit curve and result in erroneous parameters if not properly taken into account in the modeling procedure. Certainly, eclipsing binaries are also affected by long integration times, namely by a “smearing” of the eclipses so that they appear to be shallower and have a longer duration. Qualitatively, this would result in a lower inclination and larger sum of the fractional radii, while the luminosity ratio would remain unchanged, since both eclipse depths are equally affected. To quantitatively investigate the extent to which the long integration could affect the derived parameters, we generated model light curves of a typical eclipsing binary, varying its period and the sum of the fractional radii. We then binned these light curves as if they had a 29.43 minute integration time, and the same number of data points as the Q1 *Kepler* light curves. We then re-solved the light curves without accounting for the integration time, and compared the computed parameters to those used to generate the original light curve. We found that for the long-cadence *Kepler* integration time of 29.43 minutes, only systems with very low values of r_{sum} and P are significantly affected, as can be seen in Figure 3. These types of systems are less than 2% of our sample. Nevertheless, we modified the JKTEBOP program to perform a numerical integration over a given exposure time, as suggested by Kipping (2010). We tested our modifications by solving the aforementioned generated light curves, now taking the integration time into account, and successfully retrieved the inputted parameters.

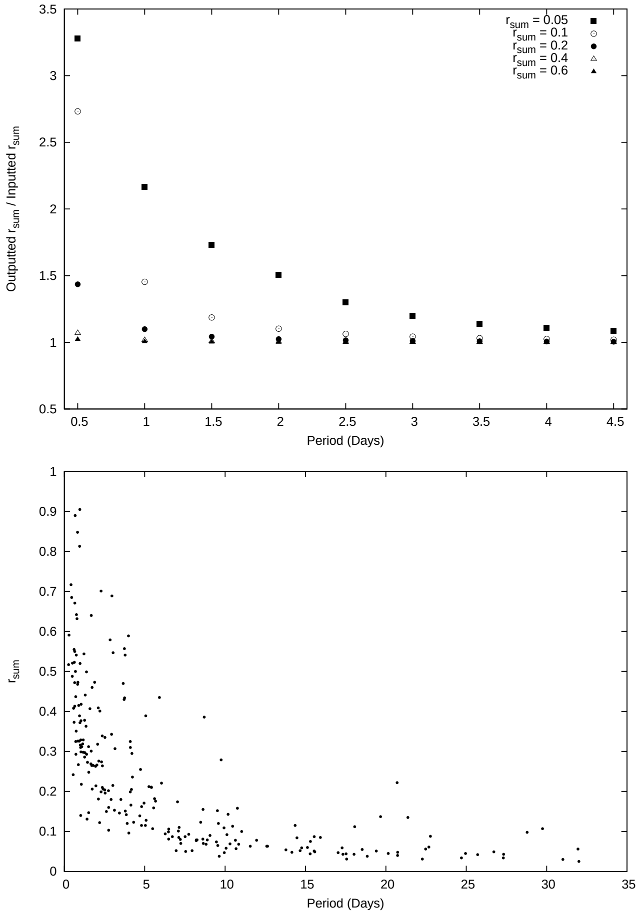

Figure 3. Top: The effect that the 29.43 minute integration time has on the derivation on the sum of the fractional radii, r_{sum}, at a given period. As can be seen, only very small values of r_{sum} and P yield discrepancies $\gtrsim$ 10%, for example, combinations of P < 3 days and $r_{sum} < 0.05$, P < 1.5 days and $r_{sum} < 0.1$, P < 0.75 days and $r_{sum} < 0.2$, etc. Bottom: The values of r_{sum} versus period for the binaries we have modeled in this paper, presented in Table 2. Very few of the systems, $\lesssim$ 2%, in our sample lie in a region where they would be significantly affected by the 29.43 minute integration time.

After estimating the individual mass, radius, and temperature for each component, we re-computed the gravity and limb-darkening coefficients for each individual star, and performed a Levenberg-Marquardt minimization starting from our previously best solutions, taking into account the 29.43 minute integration time. We then repeated the processes of deriving the physical values of the components, interpolating gravity and limb-darkening coefficients, and performing a Levenberg-Marquardt minimization several more times to ensure convergence. The JKTEBOP solutions for all initial 231 candidates are shown in Table 2, including the *Kepler* ID number, effective temperature of the system, apparent *Kepler* magnitude, magnitude range of the light curve, period, time of primary minimum, inclination, eccentricity, longitude of periastron, sum of the fractional radii, surface brightness ratio, radii ratio, luminosity ratio, amplitude of the sine curve applied to the luminosity of the primary star to account for spots, and the amount of third light. Although we list the derived surface brightness and radii ratios here, we note again that they are

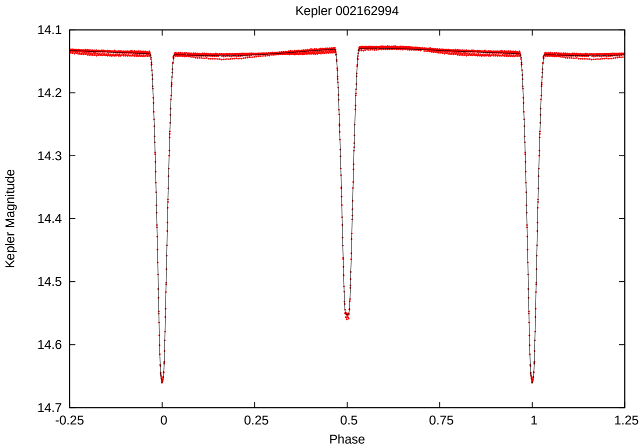

Figure 4. Plots of the light curves of the 231 systems modeled with the JKTEBOP code, presented in Table 2. Only the first plot, Figure 4.1, is shown in the text for guidance. Figures 4.1-4.231 are available in the online version of the Journal.

not always reliable on their own, and thus are combined to obtain the luminosity ratio in our analysis via Eq. 3. Plots of each of the eclipsing binaries with their model fit are given in Figure 4.

As a check on the reliability of our analysis technique we took the well-studied low-mass eclipsing binary GU Boo (López-Morales & Ribas 2005), and modeled only the R band light curve, (not using the radial velocity curves), via the exact same procedure as stated above in Sections 4 and 5. The only differences were that we used only the R-band luminosities from the Baraffe et al. (1998) and Chabrier et al. (2000) models, and an integration time of 2 minutes as stated in López-Morales & Ribas (2005). We used only the period, time of primary minimum, and estimated effective temperature of the system from broadband photometry provided in López-Morales & Ribas (2005), as we did for the systems in our main study. We find T_1 = 3912 K, M_1 = 0.61 $M_\odot$, R_1 = 0.62 $R_\odot$, T_2 = 3813 K, M_2 = 0.57 $M_\odot$, and R_2 = 0.59 via our technique. In comparison, López-Morales & Ribas (2005) found with multi-color light curves and radial-velocity curves of the system, values of T_1 = 3920 K, M_1 = 0.610 $M_\odot$, R_1 = 0.623 $R_\odot$, T_2 = 3810 K, M_2 = 0.599 $M_\odot$, and R_2 = 0.620. The values derived from our technique using only a single color light curve are accurate to within a few percent of the very precise values derived from a study using multi-color light and radial-velocity curves, thus validating our technique.

As noted above, Prša et al. (2010) estimated the parameters of temperature ratio, sum of the fractional radii, e·cos(ω), e·sin(ω), and sin(i) for detached systems, via the EBAI technique (Prša et al. 2008). Before comparing to the parameters obtained by (Prša et al. 2010), we note that the modeling approach between EBAI and our AGA presented in this paper have some fundamental differences. EBAI is extremely computationally efficient, but relies on a fitted polynomial to the actual data (Prša et al. 2008), which is then compared to a neural network training set of 33,235 light curves generated by the Wilson-Devinney code (Wilson & Devinney 1971; Wilson 1993). Prša et al. (2008) notes that "...the artificial neural network output is viable for statistical analysis and as input to sophisticated modeling engines for fine-tuning." In comparison, the use of our AGA coupled with JKTEBOP is computationally slower, but models each actual data point, obtaining an actual best-fit model while varying all physical parameters of interest over the global solution space. As well, our AGA takes into account the 29.43 minute integration time, while EBAI does not. Thus, although the EBAI technique is excellent for mining large databases, identification of light curve morphology, and obtaining estimates of parameters for statistical studies, it is not intended to model individual light curves as precisely and accurately as possible. Keeping this in mind, comparing the parameters obtained by Prša et al. (2010) to our solutions for the same systems, we first note a moderate correlation between the sum of radii given by Prša et al. (2010) and our results, with an average discrepancy of ~20%. However some of the Prša et al. (2010) solutions are unphysical, ($r_{sum} < 0.0$), and visual inspection of the polyfit curves given by Prša et al. (2010) appears to reveal a systematic underestimation of the eclipse depths. With respect to eccentricity, the parameters presented by Prša et al. (2010) reveal an unusually large number of eccentric systems, with only 3% of systems having $e \leq 0.01$, and 11% of systems with $e \leq 0.05$. In contrast, our parameters show 36% of systems with $e \leq 0.01$, and 60% of systems with $e \leq 0.05$, which better matches the large number of systems observed that do not show any offset of secondary eclipse from phase 0.5, and no difference in the eclipse widths, indicative of a circular orbit. There is only a slight correlation between our inclination values and that of Prša et al. (2010), but as we previously noted, the Prša et al. (2010) polyfit curves appear not to fit the eclipse depths well. There is practically no correlation between our values for the surface brightness ratio and EBAI's temperature ratio provided in Prša et al. (2010), though Prša et al. (2010) notes that for detached systems, the "...eclipse depth ratio is strongly affected by eccentricity and star sizes as well, rendering T_2/T_1 a poor proxy for the surface brightness ratio."

In Table 2 we list the *Kepler* ID number, orbital period, effective temperature of the system, and the estimated effective temperature, mass and radius of each stellar component for the 95 systems that contain two main-sequence stars, which we define as having a radius less than 1.5 times the Baraffe et al. (1998) and Chabrier et al. (2000) model relationships, and a light curve amplitude of at least 0.1 magnitudes, (suitable for ground-based follow-up and less likely to contain any third light). All of these 95 systems have both stars with masses less than 1.0 $M_\odot$. Note that we have ordered Table 2 such that Star 1 is always the more massive star, regardless if L_r was greater or less than 1.0 in Table 2. Also note that since we are using V+R-band luminosities, which best correspond to the *Kepler* bandpass, one cannot always use the simple $R^2 \cdot T^4$ relation to derive luminosity ratios from Table 2 to compare to Table 2, since that would correspond to the bolometric luminosity. However, if one takes a system from Table 2, looks up the V+R-band luminosity for each component, based on their mass and temperature, from the Baraffe et al. (1998) and Chabrier et al. (2000) models, and derives a luminosity ratio, this will exactly match the luminosity ratio in Table 2 from the JKTEBOP models, because the technique defines it as such. These results substantially increase the number of LMMS DDEB candidates in general, and provide 29 new LMMS DDEBs with both components below one solar mass, and at least 0.1 magnitude eclipse depths, in the heretofore unexplored period range of P > 10 days. We further discuss the impact of these systems and comparison to theoretical models in Section 7.

In Figure 5 we show an example of a system which did not meet the main-sequence criterion, Kepler 004247791, which has $T_{\rm eff}$ = 4063K and a period of 4.100866 days. If this system were main-sequence, via our method, it would have a combined mass of 1.28 $M_\odot$ and a combined radius of 3.82 $R_\odot$. This can be seen by the wide, shallow eclipses for a system of this period and effective temperature. Thus, this system contains one or two evolved stars. An additional curiosity of this system is a periodic transit-like feature that is superimposed on the eclipsing binary light curve. The transit feature occurs at just slightly less than half the orbital period of the eclipsing binary, so that it is seen twice per every revolution of the eclipsing binary system, occurring at a slightly earlier phase every revolution. We subtract the model fit from the eclipsing binary, and plot the transit feature at its period of 2.02484 days in the right panel of Figure 5. Some possible explanations may include, but are certainly not limited to: 1) a background eclipsing binary with no visible secondary eclipse at 0.49376 times the orbital period of the foreground binary, 2) a background eclipsing binary with nearly identical primary and secondary eclipses at 0.98752 times the orbital period of the foreground binary, 3) a circumbinary transiting object, or 4) a transiting object around one of the stars in an almost 2:1 resonant orbit with the binary. Follow-up multi-color light curves, spectra, and radial velocities will be needed to fully characterize this interesting system.

6. NEW TRANSITING PLANET CANDIDATES

For the 8 new transiting planet candidates mentioned in Section 3, we combined Q0 and Q1 data, and modeled the transit curves using JKTEBOP, accounting for the 29.43 minute integration time, and using our modified AGA in the same manner described in Section 4. We assumed zero eccentricity and negligible flux from each planet, and interpolated the limb-darkening and gravity-darkening coefficients via the effective temperature, surface gravity, and metallicity from the relations of Sing (2010) and Claret (2000). We then solved for the period, time of primary minimum, inclination, sum of the fractional radii, ratio of the radii, and the out of transit flux level. With this narrowed set of parameters, the AGA proved to be extremely quick and precise, and all fits were confirmed by eye and χ^2 values to accurately fit the data. Plots of the transit light curves with model fits are shown in Figure 6.

To estimate the physical radius of each transiting exoplanet candidate, we took the value for the radius of the host star from the KIC, and multiplied by the ratio of the radii, k, found from the model. In Table 2 we list the *Kepler* ID number, apparent *Kepler* magnitude, time of primary minimum, period, effective temperature of the star, inclination, radius of the star, and radius of the exoplanet candidate in both solar radii and Jupiter radii.

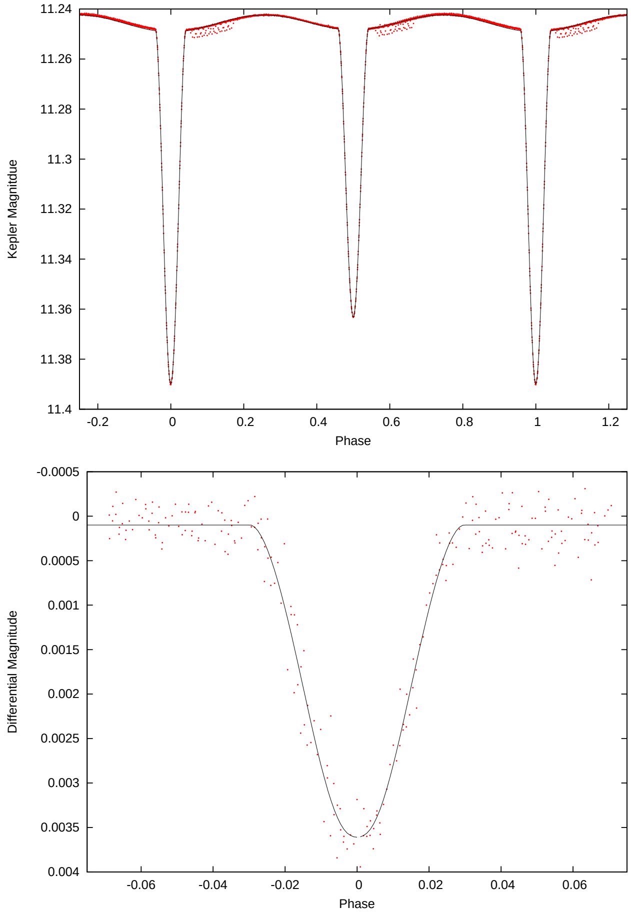

Figure 5. Kepler 004247791. An example of a system which was determined not to be main-sequence in Section 5. Top: The light curve phased at its period of 4.100866 days with our best model fit. Given the shallow, wide eclipses for a ∼4.1 day period and $T_{\rm eff}$ = 4063K, if this system were main-sequence, it would have a combined mass of 1.28 $M_\odot$ and a combined radius of 3.82 $R_\odot$. Thus, this system contains one or more evolved stars. Bottom: The model-fit subtracted light curved phased at a period of 2.02484 days, showing a transit-like feature imposed on the light curve of the eclipsing binary. Possible explanations may include, but are certainly not limited to a background eclipsing binary with no visible secondary eclipse at 0.49376 times the orbital period of the foreground binary, a background eclipsing binary with nearly identical primary and secondary eclipses at 0.98752 times the orbital period of the foreground binary, a circumbinary transiting object, or a transiting object around one of the stars in an almost 2:1 resonant orbit with the binary.

As can be seen, the radii for these transiting planet candidates range from 0.56 to 2.1 $R_{\rm Jup}$, with periods between 4.1 and 24.6 days. Only one of these, Kepler 011974540, has been ruled out as a planet from follow-up RV measurements, which are needed for the rest of the candidates to confirm or refute their planetary nature. However, even if these objects turn out not to be planetary mass, they then must be either brown dwarfs or very low-mass stars, which still are valuable finds. In the case of brown dwarfs, these targets would be located within the so-called "brown dwarf desert" (McCarthy & Zuckerman 2004).

7. COMPARISON OF THE NEW LOW-MASS BINARY CANDIDATES TO MODELS

As described in the introduction, one of the current outstanding questions in the study of low-mass stars is

Table 4
Model Parameters for the 8 Transiting Exoplanet Candidates

Kepler ID	M_{kep}	T_0 (BJD-2454900)	P (Days)	$T_{eff,\star}$ (K)	i (°)	$R_\star$ ($R_\odot$)	R_p ($R_\odot$)	R_p (R_{Jup})
001571511	13.42	68.529019	14.02065	5804	89.28	1.08	0.14	1.43
003342592	14.92	69.190452	17.17864	5717	89.20	0.93	0.14	1.37
005372966	15.37	67.675070	9.286422	5464	88.91	0.92	0.19	1.87
006756669	15.33	65.860125	5.851827	5353	88.34	0.90	0.16	1.59
006805146	13.21	56.568771	13.77974	6214	89.14	1.41	0.21	2.11
008544996	15.20	65.898818	4.081488	5463	87.61	1.00	0.13	1.27
011974540[1]	13.22	65.862352	24.67058	6507	89.53	0.69	0.06	0.56
012251650	14.76	71.657743	17.76233	4952	88.97	1.00	0.16	1.64

[1] Listed in the *Kepler* False Positive Catalog as "velocity measurements indicate eclipsing binary"

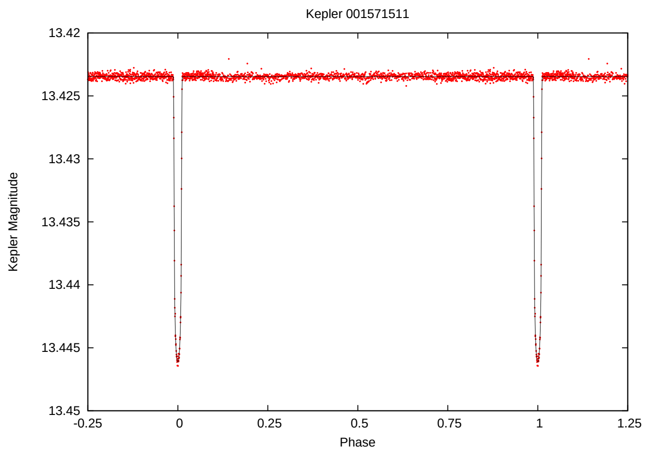

Figure 6. Plots of the light curves of the 8 transiting planet candidates modeled with the JKTEBOP code, presented in Table 2. Only the first plot, Figure 6.1, is shown in the text for guidance. Figures 6.1-6.8 are available in the online version of the Journal.

whether the inflated radii observed in binaries is caused by their enhanced stellar rotation, and therefore enhanced magnetic activity. We explore this problem in this section using the list of the 95 new LMMS DDEB candidates with estimated individual masses both below 1.0 $M_\odot$ and light curve amplitudes greater than 0.1 magnitudes, given in Table 2. This sample, for the first time, provides a statistically significant number of systems with orbital periods larger than 10 days.

The left-side panels of Figure 7 show mass-radius diagrams using the mass and radius of each binary star component estimated in Section 5. The LMMS DDEB candidates have been separated into three categories, with orbital periods $P < 1.0$ day, $1.0 < P < 10$ days, and $P > 10$ days. Each primary and secondary in a binary pair is traced by a connecting line. We also plot in each panel of Figure 7 the theoretical mass-radius relation predicted by the Baraffe et al. (1998) models for $M \geq 0.075\ M_\odot$, and the Chabrier et al. (2000) models for $M < 0.075\ M_\odot$, both for $[M/H] = 0.0$, and an age of 5.0 Gyrs. We have also defined a main-sequence cutoff as 1.5 times the theoretical mass-radius relation, which is illustrated by the solid line in each diagram. In the models we have used an $\alpha = 1.0$ for $M \leq 0.7\ M_\odot$ and interpolated the radius of the models for $0.7\ M_\odot < M \leq 1.0\ M_\odot$ by fixing the radius of the 1.0 $M_\odot$ model to 1.0 $R_\odot$, therefore avoiding the dependence of the stellar radius with α between 0.7 $M_\odot$ and 1.0 $M_\odot$ (Baraffe et al. 1998). We also include in the mass-radius diagrams estimations of the error in our M and R values at several masses, computed by adding and subtracting 200 K, (the error in the T_{eff} determinations given by the KIC), from a given temperature and interpolating the mass and radius from the theoretical relations. Note that one of the long-period stars, Kepler 008075618, falls well below the main-sequence, with two identical components with $M = 0.91\ M_\odot$ and $R = 0.53\ R_\odot$. Inspection of this light curve, coupled with the light curve model, reveals that this system could in fact be a single-lined system at half the listed period.

In the figure, many of the stellar radii of binaries with $P < 1.0$ days appear to fall above the model predictions, but as the orbital period increases, a larger fraction of the systems appear to have radii that are either consistent with or fall below the models. There certainly is a fair amount of scatter in these data introduced by the large error in the mass and radius estimations, but a histogram analysis of the radius distributions confirms these apparent trends. On the right-side panels of Figure 7 we show 5% bin-size histograms representing how many stars have a radius that deviates by a given percentage from the models. The average radius discrepancy is 13.0%, 7.5%, and 2.0% for the short ($P < 1.0$ days), medium ($1.0 < P < 10.0$ days), and long-period ($P > 10.0$ days) systems respectively. Although a full analysis of each system with multi-color light and radial-velocity data is still needed, these preliminary estimates support the hypothesis that binary spin-up is the primary cause of inflated radii in short period LMMS DDEBs.

8. SUMMARY

We present 231 new double-eclipse, detached eclipsing binary systems with $T_{eff} < 5500$ K, found in the Cycle 0 data release of the *Kepler Mission*, and provide their *Kepler* ID, estimated effective temperature, *Kepler* magnitude, magnitude range of the light curve, orbital period, time of primary minimum, inclination, eccentricity, longitude of periastron, sum of the fractional radii, and luminosity ratio. We estimate the masses and radii of the stars in these systems, and find that 95 of them contain two main-sequence stars with both components having $M < 1.0\ M_\odot$ and eclipse depths of at least 0.1 magnitude, and thus are suitable for ground-based follow-up. Of these 95 systems, 14 have periods less than 1.0 day, 52 have periods between 1.0 and 10.0 days, and 29 have periods greater than 10.0 days. This new sample of low-mass, double-eclipse, detached eclipsing binary candidates more than doubles the number of

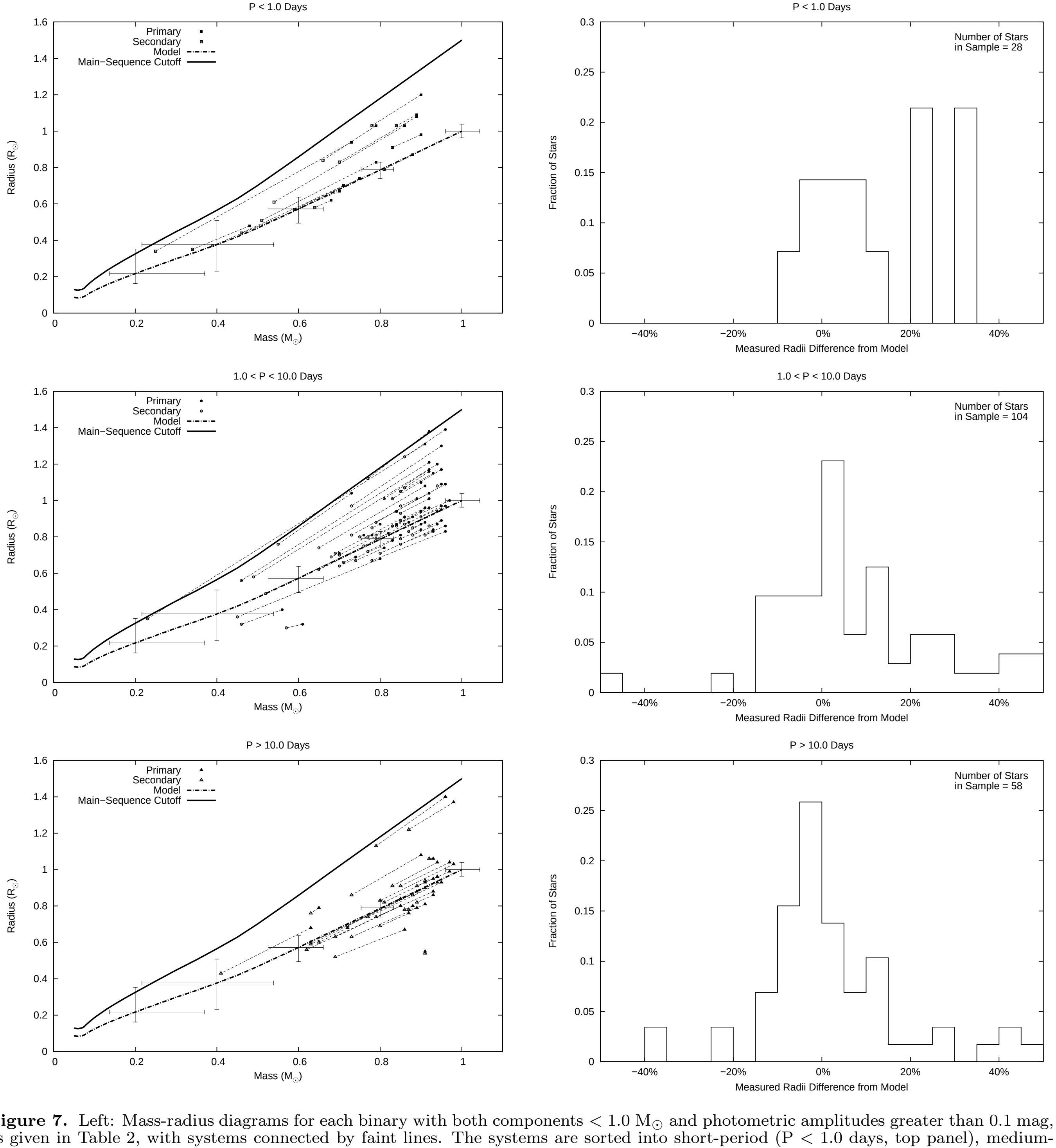

Figure 7. Left: Mass-radius diagrams for each binary with both components < 1.0 M$_\odot$ and photometric amplitudes greater than 0.1 mag, as given in Table 2, with systems connected by faint lines. The systems are sorted into short-period (P $<$ 1.0 days, top panel), medium-period, (1.0 $<$ P $<$ 10.0 days, middle panel), and long-period groupings, (P $>$ 10.0 days, bottom panel). The theoretical mass-radius relations of Baraffe et al. (1998) for 0.075 M$_\odot$ $\leq$ M $\leq$ 1.0 M$_\odot$, and of Chabrier et al. (2000) for M $<$ 0.075 M$_\odot$, both for [M/H] = 0.0 and an age of 5.0 Gyr, are over-plotted. The solid line shows the main-sequence cutoff criterion. The error bars indicate the error in mass and radius obtained when interpolating from the mass-temperature-radius relations with an error of 200K. Right: Histograms of the fraction of stars in the sample versus their deviance from the models for each period grouping. As can be seen by both the mass-radius relation plots and the histograms, shorter period binaries in general appear to exhibit larger radii compared to the models than longer period systems.

previously known systems, and extends the sample into the completely heretofore unexplored P > 10.0 day period range for LMMS DDEBs.

Comparison to the theoretical mass-radius relation models for stars below 1.0 $M_\odot$ by Baraffe et al. (1998) show preliminary evidence for better agreement with the models at longer periods, where the rotation rate of the stars is not expected to be spun-up by tidal locking, although, in the absence of radial-velocity measurements, the errors on the estimated mass and radius are still quite large. For systems with P < 1.0 days, the average radius discrepancy is 13.0%, whereas for 1.0 < P < 10.0 days and P > 10.0 days, the average radius discrepancy is 7.5% and 2.0%, respectively. Ground-based follow-up, in the form of radial velocity and multi-wavelength light curves, is needed to derive the mass and radius of each star in each system to ∼1-2%, which we have already begun to acquire. With accurate masses and radii for multiple long-period systems, we should be able to definitively test the hypothesis that inflated radii in low-mass binaries are principally due to enhanced rotation rates.

We also present 8 new transiting planet candidates. Only one of them is currently listed in the *Kepler* False Positive Catalog. The remaining candidates require radial-velocity follow-up to confirm or refute their planetary nature. Even if these systems do not turn out to be planets, they then must be brown dwarf or very low-mass, late-type M dwarfs, which would still be a very valuable find. In fact, all false positive planet candidates determined by the *Kepler* team will be of great interest to stellar astrophysics. We also present 7 new extremely shallow eclipsing systems, one well detached binary with deep eclipses, and one apparent red giant with an unusual eclipse-like feature. We also highlight a very unusual eclipsing binary system containing at least one evolved star and an additional transit-like feature in the light curve. Finally, the systems that we determined are not main-sequence, and we therefore did not include in the subsequent analysis, should be further studied for valuable science. Accurate mass, radius, and temperature determinations of those systems could yield valuable insights into stellar and binary evolution.

Acknowledgements

We first and foremost thank the entire *Kepler* team and all those who have contributed to the *Kepler Mission*, without which this paper would not be possible. We also thank our second referee for a very thorough and helpful review. J.L.C acknowledges support from a NSF Graduate Research Fellowship and the New Mexico Space Grant Consortium. J.L.C., M.L.M., & T.E.H. are grateful for funding from *Kepler's* Guest Observer Program. M.L.M. acknowledges support from NASA through Hubble Fellowship grant HF-01210.01-A/HF-51233.01 awarded by the STScI, which is operated by the AURA, Inc. for NASA, under contract NAS5-26555. We also thank Robert Edmonds at New Mexico State University for inspiring us to modify the AGA to use a Gaussian distribution to create new individuals. Some/all of the data presented in this paper were obtained from the Multimission Archive at the Space Telescope Science Institute (MAST). STScI is operated by the Association of Universities for Research in Astronomy, Inc., under NASA contract NAS5-26555. Support for MAST for non-HST data is provided by the NASA Office of Space Science via grant NNX09AF08G and by other grants and contracts. This research has made use of NASA's Astrophysics Data System.

APPENDIX

A. ECLIPSE PHASE DISPERSION MINIMIZATION (EPDM)

In this appendix we further explain the EPDM technique introduced in Section 3. As mentioned in the text, EPDM finds the period of an eclipsing binary system by seeking the value of the period that best minimizes the dispersion in phase of the faintest N points in a light curve. To illustrate how this methods works, we show in Figure 8 the period search analysis of the LMMS DDEB candidate Kepler 006591789, which was found to have a period of 5.088435 days via the JKTEBOP model, (see Table 2). The unfolded Q1 light curve is shown in the top-left panel of Figure 8. EPDM selects the faintest 20 points of the light curve, which are highlighted by the larger points in that same panel. The number of points should be adjusted based on the quality of the data set. Too few points could result in all the points selected belonging to the same eclipse, if that one eclipse is unusually deep due to systematics or another reason, and thus EPDM will be unable to determine a period. Too many points will cause the results of EPDM to be less precise, as more points are included further away from the center of the eclipses. We have found that 20 points is a good number for *Kepler* data, for which many systems do suffer from moderate systematics, as is evidently the case for Kepler 006591789, as seen by the quasi-sinusoidal variation in the baseline flux.

Having selected the faintest points from the light curve, EPDM then loops over a range of period values. In this case we choose a set of 5,000 period values that range from 0.3 to 30 days, evenly distributed in log space, so that shorter periods are as well-sampled as longer periods. At each period, the phase of each of the 20 faintest points are calculated via the following standard equation,

$$p = \frac{T}{P} - int(\frac{T}{P}) \tag{A1}$$

where p is the phase of a given point, with a time value, T, for a given period, P, and int() returns the argument rounded down to the nearest integer value. The standard deviation of these 20 phase values is then computed, and we are left with a standard deviation for each trial period. In the bottom-left panel of Figure 8, we plot the standard deviation in phase of the 20 points versus each trial period. The lowest values for the standard deviation indicate the best periods, where the eclipses align in phase-space, while high values indicate bad periods. As can be seen in the bottom-left panel, the standard deviation approaches a value of 0.0 near 10.2 days, 5.1 days, 2.05 days, and decreasing

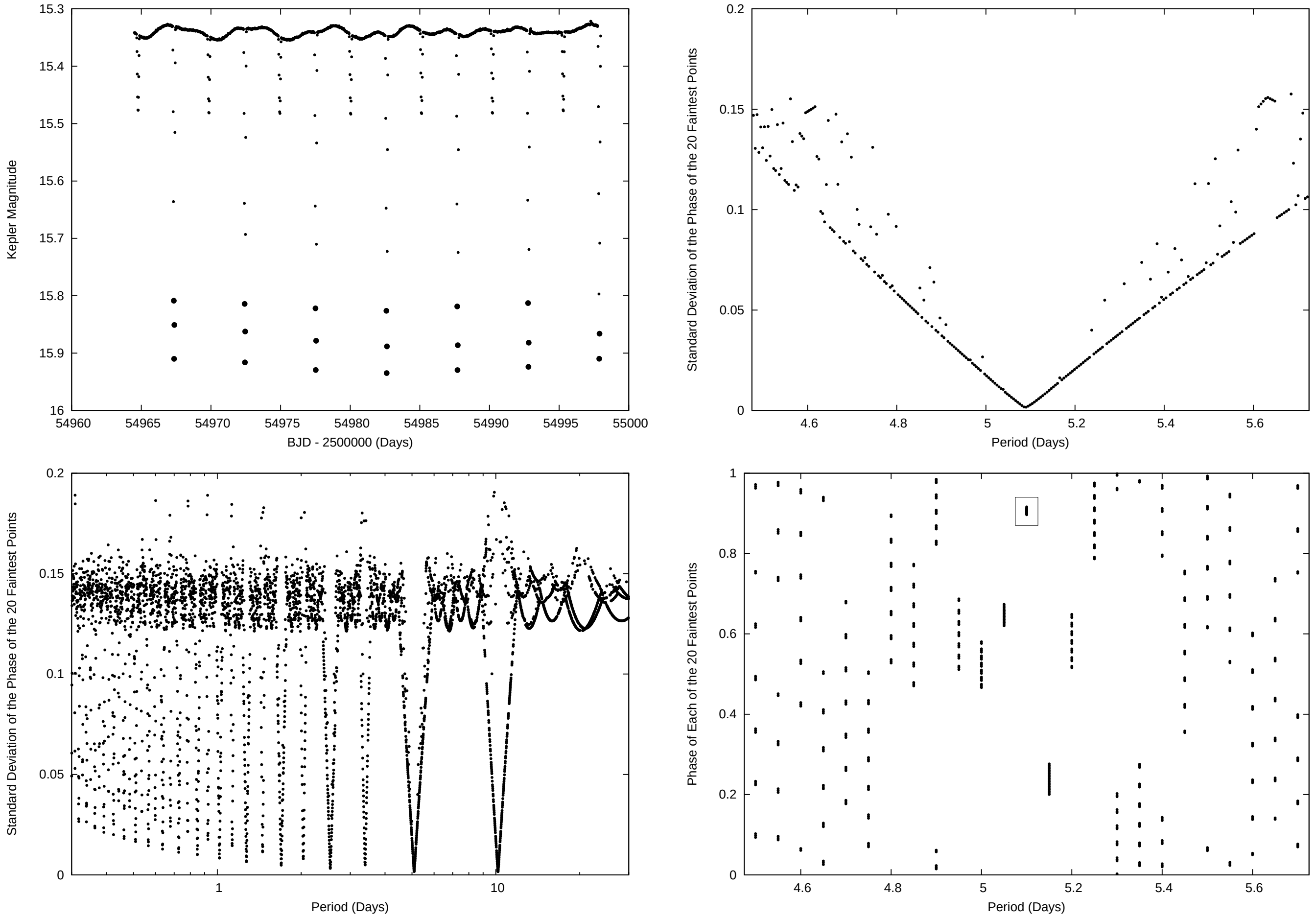

Figure 8. Illustration of the EPDM technique. Top-left: The unphased light curve of Kepler 006591789, with the 20 faintest points highlighted by using larger point sizes. Bottom-left: Standard deviation of the phase values of the 20 faintest points versus period for this system. As can be seen, the standard deviation approaches 0.0 at ∼5.1 days, and integer multiples and fractions thereof. Top-Right: The same plot as in the bottom-left panel, but with the period range restricted to show only the period with the lowest standard deviation, and true period of the system. Bottom-Right: The actual phase values for each of the 20 faintest points at multiple periods, spanning the same period range, (but with a lower period resolution, for clarity), as the plot in the top-right panel. As can be seen, as the examined period approaches the true period of the system, the phase values of the 20 faintest points strongly clump together, producing a very small standard deviation. The best period is highlighted by a box in the lower-right panel.

fractions thereof, or period aliases. To determine the three best periods, EPDM first selects the lowest standard deviation, which in this case yields a value of 5.09004 days. It then selects the next lowest value, whose corresponding period value differs from the first by at least 10%, and yields a value of 10.1747 days. The third period selected via the same method yields a value of 2.54402 days.

To further clarify the technique visually, in the top-right panel of Figure 8, we show the same plot as in the bottom-left panel, but limited in period range to straddle the best period found, 5.09004 days. At the same period range, in the bottom-right panel, we plot the actual values of the phase for each of the 20 points at each period. (For ease of viewing, we use a lower trial period resolution in the bottom-right panel than the top-right panel.) As can be seen in the lower-right panel, when the trial period is far from the true period of the system, the actual phase values have a large dispersion, and range completely from 0.0 to 1.0. As the given period gets closer to the true period, the phase values begin to clump, with their dispersion decreasing as the trial period approaches the true value. Indeed, as highlighted by the box in the bottom-right panel of Figure 8, at the best period, all the phase values are tightly grouped together at P = 5.0904 days, indicating that all the eclipses are extremely well aligned, and the period of the system has been found.

One complication that can arise is if EPDM encounters an eccentric system with two similarly deep eclipses. In this case, when the algorithm selects the N faintest points, it will be selecting points from both eclipses. Since the system is eccentric, there is a phase offset not equal to 0.5 between primary and secondary eclipse, i.e. the two eclipses occur closer to each other in time compared to the period of the system. In this case, if we were to run EPDM as just described, in a plot like the bottom-right panel of Figure 8, at the true period of the system there would be two groups of points, each by itself having a very small deviation, but separated from each other in phase by a large amount. Thus, the standard deviation calculation will show a much higher value than it should, and the correct period could not be found. Along similar lines, a problem arises when we consider how to calculate the standard deviation of, for example, the distribution of phase points in the bottom-right panel of Figure 8 at a period of 4.9 days, which ranges from 0.8 - 1.0, and then jumps to 0.0 - 0.05. It is clear this is a continuous group of points, which simply experiences an abrupt jump from phase 1.0 to 0.0. Although they represent a fairly good period, a calculation of their standard deviation would show a high value, and thus indicate a bad period.

To reconcile both these problems, we insert an additional step into the EPDM technique. At each trial period, EPDM searches for a reflection phase, p_r, whose value is between 0.0 and 1.0, that will allow the two distinct phase groupings to align. For each value of p_r, if the phase value of a given point is larger than p_r, a new value for the phase of the point, p, is calculated as

$$p = p - 2.0 \cdot (p - p_r) \tag{A2}$$

The value of p_r which yields the lowest standard deviation for a given trial period is the correct reflection value, and that corresponding lowest standard deviation should be assigned to that trial period. Thus, in the case of an equal depth, eccentric system, where say the N lowest points group around two phases of 0.2 and 0.4, at a value of p_r = 0.3, the two distinct groupings would merge into a single group at phase 0.2, with a very small standard deviation at the correct period of the system. As well, in the case where a group of phase points that range from 0.9 to 1.0 and 0.0 to 0.1, p_r allows the points to merge into a single group that only ranges from 0.0 to 0.1. In fact, we have already implemented the use of p_r when generating the bottom-left and top-right plots of Figure 8.

In conclusion, because EPDM only utilizes the faintest N points of a light curve, the computations are very quick, especially compared to traditional phase dispersion minimization techniques, which utilize every point in a light curve. This also allows for a more precise determination of the period, as one can apply more computing time towards finer period resolution. As well, for the same reason, EPDM is not affected by systematics or varying star spots, as long as their photometric amplitudes are not on the order of or greater than the amplitude of the eclipses. By selecting the faintest point, or the earliest of the N faintest points, one is also given a good value for the time of primary minimum. We have shown EPDM can be applied to both eccentric and non-eccentric binaries, and since a transiting planet's light curve is similar to an eclipsing binary with only one visible eclipse, the technique works equally well for transiting exoplanets. In theory, EPDM could also be applied to other variables, such as stars with rotating spots, pulsating variables, and contact binaries, although periods for these systems will be less precise than detached eclipsing binaries, due to the broader minima of those systems. In theory though, one may not have to select the faintest points of a light curve, but possibly a very narrow flux range, and achieve the same result.

B. GENETIC ALGORITHMS FOR ECLIPSING BINARIES

As mentioned in the text, in fitting our sample of eclipsing binaries, we have 12 parameters: period, time of primary minimum, inclination, mass ratio, e·cos(ω), e·sin(ω), surface brightness ratio, sum of the fractional radii, ratio of the radii, out of eclipse flux level, and the amplitude and phase shift of the sinusoid applied to the luminosity of the primary in order to account for spots. We aim to vary these parameters over their entire range of possible solutions, which if left to a grid search for 10^{-3} precision, would require computing on the order of $\sim 10^{36}$ light curves; a computationally prohibitive task. Standard steepest descent minimization schemes such as Levenberg-Marquardt have extreme difficulties in large, multi-parameter solution spaces, especially for eclipsing binaries as the solution space is not at all smooth and has many local minima. Thus, we need a minimization technique that is computationally efficient, not adversely affected by a non-smooth solution space, and able to find the global minimum. These criteria are superbly met by the class of optimization schemes known as Genetic Algorithms (GAs).

In a standard GA, (cf. Charbonneau 1995), light curve parameter sets, called individuals, for an initial population of solutions, are randomly generated within a predefined parameter space, and compared to the observational light curve. Their corresponding χ^2 value is used as a measure of fitness for natural selection, with parameters from fit individuals bred with each other, (subjected to crossover like chromosomes), to create a second generation of new solutions, and parameters from unfit individuals eliminated. After being subject to random mutations, to maintain parameter diversity and ensure discovery of the global minimum, this second generation is compared to the observational data, and bred into a third generation of solutions. The process continues for a specified number of generations, until a satisfactorily low χ^2 is found. Charbonneau (1995) demonstrated the application of GAs to problems in Astronomy and Astrophysics, specifically fitting galactic rotation curves, finding pulsation periods in δ Scuti stars, and fitting magnetodynamical wind models with multiple critical points, showing how the GA quickly finds the global minimum, regardless of the topography of the solution space. It is this type of GA that has been already been incorporated into the ELC eclipsing binary modeling code, and used with much success (Orosz & Hauschildt 2000; Orosz et al. 2002).

Cantó et al. (2009) recently proposed a new form of GA called an Asexual Genetic Algorithm (AGA). In the AGA, instead of breeding new individuals via crossover, individuals are randomly created within a small predefined parameter space, or breeding box, centered on the fittest members of the previous generation. The size of this breeding box can be shrunk over successive generations to quickly converge to the best-fit solution. As shown by Cantó et al. (2009), the AGA is computationally simpler and more precise since it does not require encoding parameters for crossover, and converges much faster than traditional GAs, without sacrificing any ability to migrate to the global solution, so long as the breeding box size does not decrease too quickly. Cantó et al. (2009) first showed that it far outperformed the standard GA in both computational efficiency and final precision by solving one of the exact same problems presented by Charbonneau (1995). Cantó et al. (2009) additionally demonstrated the application of the AGA to fitting the radial-velocities of extrasolar planets and the spectral energy distributions of young stellar objects.

As eclipsing binary solutions have an even larger parameter space with many local minima than most problems, we make a few modifications to the AGA described by Cantó et al. (2009) to ensure discovery of the global minimum. First, while we do exactly copy the fittest 10% of individuals of one generation to the next generation, to ensure forward progress is always made while maintaining parameter diversity, instead of picking the fittest N members of a generation, each of which breeds M offspring, to create a new generation, we randomly select individuals for breeding by weighting them by a factor of $(1/\chi^2)^2$. This ensures that the fittest individuals breed the most offspring, but still allows for a few less fit individuals to breed, maintaining parameter diversity and exploration of the entire parameter space. Second, instead of randomly creating new members within a breeding box of fit individuals, we randomly select a number for each parameter from a Gaussian probability distribution centered on each parameter of a fit individual. Thus, new individuals are not strictly confined to a breeding box, but merely are very likely to be created near a fit individual, and maintain a very small probability that they will be created at many standard deviations away. This mimics mutation in traditional GAs and ensures that the algorithm will not become trapped in a local minimum. Third, as suggested by Cantó et al. (2009), the standard deviation of this normal distribution is chosen for each parameter to be the standard deviation of that parameter in the entire population, times the function $0.1^{(1/\chi_0^2)}$, where χ_0^2 is the χ^2 value of the fittest member of the population. This allows parameters with the greatest impact on the fit, or the smallest range of possible parameters, such as the out of eclipse flux level, to converge rapidly, while allowing parameters that are less certain to converge more slowly and thoroughly explore their parameter space. Furthermore, via this method, the standard deviation is shrunk over successive generations, so that the algorithm converges, but only very slowly initially, rapidly increasing as χ_0^2 approaches 1.0, i.e. the global minimum has been found. Finally, we take the fittest 10% of the final generation and perform a standard Levenberg-Marquardt minimization for each member, choosing the member with the resulting lowest χ^2 value as our final solution.

We nominally found, for the eclipsing binaries in our sample, that a population of 100 individuals, bred for 200 generations, does an excellent job of solving the light curves. This only requires the generation of 20,000 light curves, which with the JKTEBOP code only required ∼3 minutes per light curve to solve on a single 2.0 GHz CPU. Of course, some systems may require a smaller or greater number of individuals and/or generations, but it should not be more than a factor of ∼2. One may substantially reduce the number of individuals or generations required, and thus the run time, if one can limit the range of parameter space. For example, if one knows, or wants to assume, the orbit is circular or nearly circular, one could constrain $|e\cdot\cos(\omega)| < 0.1$ and $|e\cdot\sin(\omega)| < 0.1$. Furthermore, the AGA code is extremely parallelizable, and thus with a multi-core computing cluster one could easily use this technique to model thousands of eclipsing binary lightcurves, as is to be expected from Pan-STARRS and other large photometric surveys, in a very reasonable time frame.

To visually demonstrate how the AGA works, we have generated a light curve with the following parameters: $r_{sum} = 0.25$, $k = 1.1$, $i = 89.0°$, $q = 1.2$, $e\cdot\cos(\omega) = 0.1$, $e\cdot\sin(\omega) = -0.1$, $J = 1.1$, $P = 2.20$ days, $T_0 = 312.3$ days, and out of eclipse magnitude = 13.5. We then re-bin this data to match the number of data points in the Kepler Q1 data sets, and add typical Gaussian noise for a bright Kepler star of 0.1 mmag per data point. We then re-solve this light curve with the AGA, varying all the aforementioned parameters, and show in Figure 9 the value of each parameter for every individual in each generation, as well as the values for the derived reduced χ^2 and luminosity ratio. One can see how even while searching over the entire global solution space, the AGA rapidly converges to the solution that was used to generate the light curve, with the χ^2 decreasing by a factor of ∼10 every ∼20 generations. Even though the best solution of the 200^{th} generation has $\chi^2 \sim 1.5$, if allowed to continue for more generations, this run would eventually converge to $\chi^2 = 1.0$, and performing a simple Levenberg-Marquardt minimization from the best solution quickly produces a $\chi^2 = 1.0$ fit.

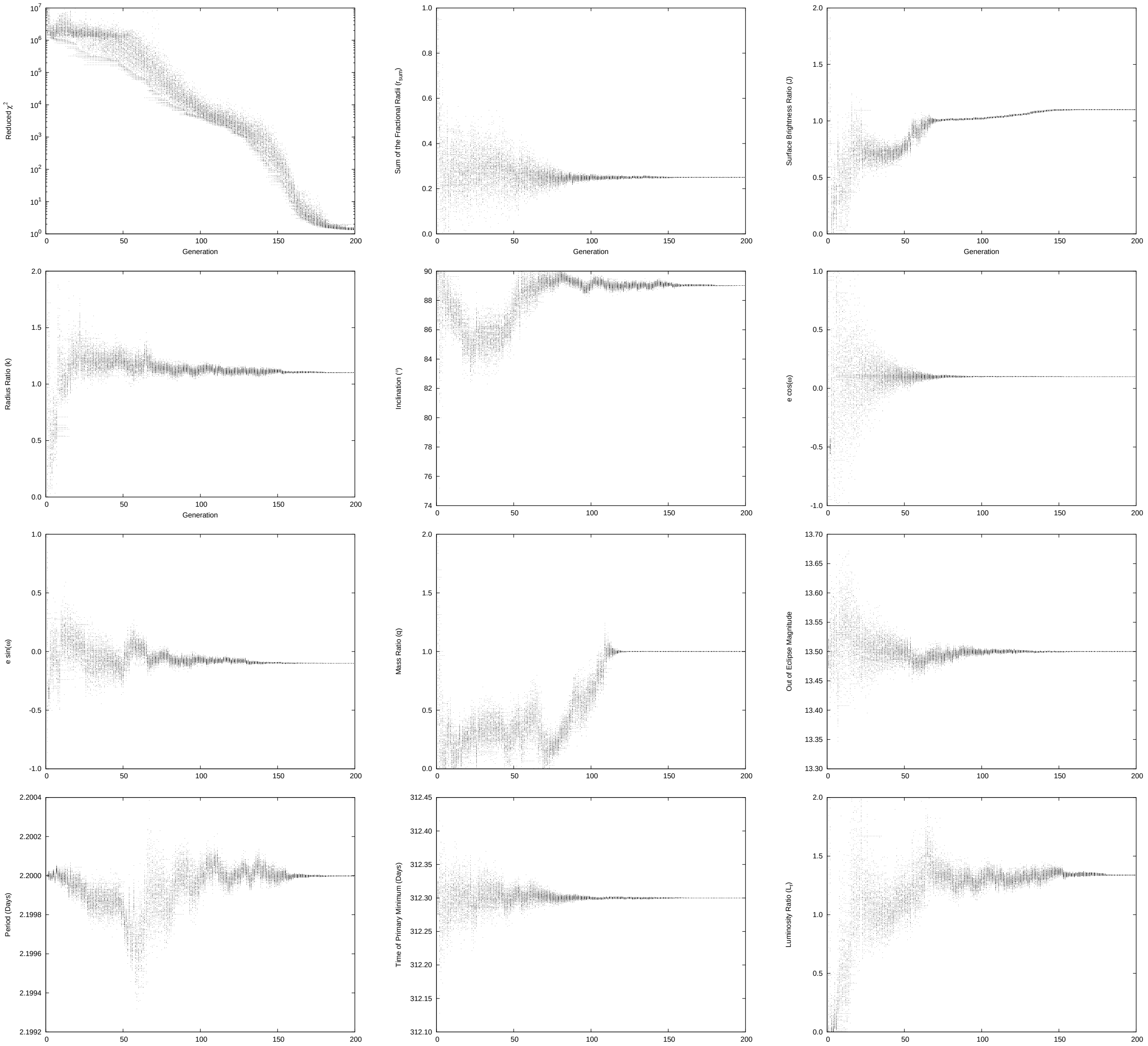

Figure 9. Illustration of how the AGA converges over subsequent generations by solving an artificially generated light curve, re-binned to the number of data points and error typical for a *Kepler* light curve. The parameters of the system are r_{sum} = 0.25, k = 1.1, i = 89.0°, q = 1.2, e·cos(ω) = 0.1, e·sin(ω) = -0.1, J = 1.1, P = 2.20 days, T_0 = 312.3 days, and out of eclipse magnitude = 13.5. The derived reduced χ^2 and luminosity ratio are also plotted. The AGA converges rapidly, decreasing the lowest χ^2 value found by an order of magnitude every ~20 generations. It can be seen that the parameters that are most significant to the light curve converge the fastest.

REFERENCES

Andersen, J. 1991, A&A Rev., 3, 91

Baraffe, I., Chabrier, G., Allard, F., & Hauschildt, P. H. 1998, A&A, 337, 403

Becker, A. C., et al. 2008, MNRAS, 386, 416

Blake, C. H., Torres, G., Bloom, J. S., & Gaudi, B. S. 2008, ApJ, 684, 635

Borucki, W. J., & the Kepler Team. 2010, ArXiv e-prints, 1006.2799

Boyajian, T. 2010 (Presentation at Cool Stars 16 in Seattle, WA)

Cantó, J., Curiel, S., & Martínez-Gómez, E. 2009, A&A, 501, 1259

Chabrier, G., Baraffe, I., Allard, F., & Hauschildt, P. 2000, ApJ, 542, 464

Chabrier, G., Gallardo, J., & Baraffe, I. 2007, A&A, 472, L17

Charbonneau, P. 1995, ApJS, 101, 309

Claret, A. 2000, A&A, 359, 289

Claret, A., & Gimenez, A. 1990, A&A, 230, 412

Clausen, J. V., Bruntt, H., Claret, A., Larsen, A., Andersen, J., Nordström, B., & Giménez, A. 2009, A&A, 502, 253

Coughlin, J. L., & Shaw, J. S. 2007, Journal of the Southeastern Association for Research in Astronomy, 1, 7

Delfosse, X., Forveille, T., Mayor, M., Burnet, M., & Perrier, C. 1999, A&A, 341, L63

Demory, B., et al. 2009, A&A, 505, 205

Devor, J., Charbonneau, D., O'Donovan, F. T., Mandushev, G., & Torres, G. 2008a, AJ, 135, 850

Devor, J., et al. 2008b, ApJ, 687, 1253

Dimitrov, D. P., & Kjurkchieva, D. P. 2010, MNRAS, 866

Fernandez, J. M., et al. 2009, ApJ, 701, 764

Hoffman, D. I., Harrison, T. E., Coughlin, J. L., McNamara, B. J., Holtzman, J. A., Taylor, G. E., & Vestrand, W. T. 2008, AJ, 136, 1067

Irwin, J., et al. 2009, ApJ, 701, 1436

Kinemuchi, K., Smith, H. A., Woźniak, P. R., & McKay, T. A. 2006, AJ, 132, 1202

Kipping, D. M. 2010, MNRAS, 1184

Lacy, C. H. 1977, ApJ, 218, 444

Leung, K., & Schneider, D. P. 1978, AJ, 83, 618

López-Morales, M. 2007, ApJ, 660, 732

López-Morales, M., & Ribas, I. 2005, ApJ, 631, 1120

Manduca, A., Bell, R. A., & Gustafsson, B. 1977, A&A, 61, 809

McCarthy, C., & Zuckerman, B. 2004, AJ, 127, 2871

Morales, J. C., Gallardo, J., Ribas, I., Jordi, C., Baraffe, I., & Chabrier, G. 2010, ApJ, 718, 502

Morales, J. C., Ribas, I., & Jordi, C. 2008, A&A, 478, 507

Orosz, J. A., & Hauschildt, P. H. 2000, A&A, 364, 265

Orosz, J. A., et al. 2002, ApJ, 568, 845

Popper, D. M. 1980, ARA&A, 18, 115

Prša, A., Guinan, E. F., Devinney, E. J., DeGeorge, M., Bradstreet, D. H., Giammarco, J. M., Alcock, C. R., & Engle, S. G. 2008, ApJ, 687, 542

Prša, A., et al. 2010, ArXiv e-prints, 1006.2815

Rowe, J. F., et al. 2010, ApJ, 713, L150

Shaw, J. S., & López-Morales, M. 2007, in Astronomical Society of the Pacific Conference Series, Vol. 362, The Seventh Pacific Rim Conference on Stellar Astrophysics, ed. Y. W. Kang, H.-W. Lee, K.-C. Leung, & K.-S. Cheng, 15

Shkolnik, E., Liu, M. C., Reid, I. N., Hebb, L., Cameron, A. C., Torres, C. A., & Wilson, D. M. 2008, ApJ, 682, 1248

Shkolnik, E. L., Hebb, L., Liu, M. C., Reid, I. N., & Cameron, A. C. 2010, ApJ, 716, 1522

Sing, D. K. 2010, A&A, 510, A21

Southworth, J., Maxted, P. F. L., & Smalley, B. 2004a, MNRAS, 351, 1277

Southworth, J., Zucker, S., Maxted, P. F. L., & Smalley, B. 2004b, MNRAS, 355, 986

Stellingwerf, R. F. 1978, ApJ, 224, 953

—. 2006, PDM2 Application, Technical Manual, and test data sets

Torres, G., Andersen, J., & Giménez, A. 2010, A&A Rev., 18, 67

Torres, G., Lacy, C. H., Marschall, L. A., Sheets, H. A., & Mader, J. A. 2006, ApJ, 640, 1018

Van Cleve, J. 2010, Kepler Data Release 5 Notes, NASA Ames Research Center, Moffett Field, CA

Wade, R. A., & Rucinski, S. M. 1985, A&AS, 60, 471

Wilson, R. E. 1993, in Astronomical Society of the Pacific Conference Series, Vol. 38, New Frontiers in Binary Star Research, ed. K.-C. Leung & I.-S. Nha, 91–+

Wilson, R. E., & Devinney, E. J. 1971, ApJ, 166, 605

Zahn, J. 1977, A&A, 57, 383

—. 1994, A&A, 288, 829

Table 2
Model System Parameters via JKTEBOP for the 231 DDEBs with $T_{\rm eff}$ < 5500 K

Kepler ID	$T_{\rm eff}$ (K)	$m_{\rm kep}$	$\Delta m_{\rm kep}$	Period (Days)	T_0 (BJD-2450000)	i (°)	e^1	ω^1 (°)	$r_{\rm sum}$	J	k	L_r	L_1 Sine Amplitude	L_3
002162994	5410	14.162	0.535	4.101544	5002.545861	89.87	0.01	270	0.199	0.991	0.702	0.4888	0.008	0.00
002437452	5398	16.981	0.256	14.47184	5003.759350	87.46	0.08	90	0.084	0.641	2.47	3.905	0.011	0.00
002580872	5293	14.880	0.374	15.92672	4978.550988	87.95	0.26	102	0.084	1.14	1.25	1.774	0.014	0.00
002719873	5086	15.160	0.235	17.27953	4968.273250	87.76	0.31	90	0.059	0.633	2.64	4.425	0.007	0.00
002852560	5381	15.308	0.460	11.96119	4964.912794	88.06	0.44	41	0.079	1.04	0.986	1.008	0.000	0.00
002860788	5319	14.043	0.137	5.259798	4965.066945	82.29	0.00	268	0.212	0.876	0.561	0.2755	0.009	0.00
003003991	5366	13.926	0.115	7.244790	4964.859062	86.88	0.28	270	0.083	0.0438	11.2	5.447	0.000	0.40
003102024	5117	12.809	0.351	13.78248	4958.697309	89.50	0.54	302	0.054	0.605	1.37	1.138	0.000	0.43
003113266	5077	15.577	0.011	0.9958567	5002.193202	72.96	0.01	266	0.325	1.24	9.95	123.3	0.026	0.00
003241344	5422	14.756	0.401	3.912656	4966.427889	90.00	0.02	256	0.121	0.0854	0.509	0.02209	0.012	0.00
003241619	5165	12.524	0.802	1.703368	4965.468231	85.35	0.03	88	0.267	0.303	1.04	0.3286	0.016	0.00
003344419	5348	14.997	0.005	0.6517609	4977.843744	50.18	0.01	269	0.694	1.08	23.4	592.4	0.068	0.00
003458919	5063	13.815	0.121	0.8920383	5002.281060	73.06	0.14	270	0.418	0.362	3.95	5.653	0.056	0.00
003543270	5288	15.220	0.130	4.177213	5003.789822	82.27	0.05	269	0.207	0.254	0.394	0.03937	0.024	0.00
003556742	4921	14.221	0.004	0.8229667	5003.017211	37.02	0.00	247	0.848	2.41	15.5	576.3	0.108	0.00
003656322	5075	13.061	0.150	3.660009	4989.330479	67.54	0.02	125	0.457	0.930	1.66	2.576	0.125	0.00
003730067	4099	14.610	0.594	0.2940818	4964.591764	75.71	0.03	88	0.590	0.420	1.25	0.6522	0.035	0.00
003830820	3902	15.368	0.044	15.58263	4999.277480	87.92	0.47	79	0.057	2.39	2.10	10.57	0.000	0.60
003834364	5449	14.661	0.089	2.908455	4965.315292	82.21	0.10	271	0.182	0.0407	0.874	0.03106	0.006	0.00
003848919	5226	13.901	0.636	1.047253	4964.766251	85.07	0.00	84	0.418	0.903	1.04	0.9684	0.017	0.00
003957477	5395	12.477	0.073	0.9789470	4964.726279	66.89	0.03	91	0.525	1.42	2.97	12.52	0.055	0.00
004049124	5349	14.654	0.175	4.804341	4969.004205	84.04	0.41	89	0.160	1.32	2.24	6.592	0.002	0.00
004077442	4523	13.512	0.153	0.6928736	5002.273033	69.03	0.01	277	0.499	1.94	1.34	3.499	0.183	0.00
004078693	5288	13.485	0.005	2.756407	5001.858784	85.40	0.32	270	0.119	0.0308	0.519	0.008294	0.001	0.79
004247791	4063	11.260	0.152	4.100862	5001.145258	77.90	0.00	87	0.326	0.928	1.48	2.035	0.001	0.00
004281895	5309	12.256	0.078	9.543591	5002.358654	87.52	0.30	4	0.065	1.18	3.41	13.80	0.000	0.00
004346875	5339	15.584	0.284	4.694341	5004.332965	87.08	0.02	267	0.135	0.0866	0.429	0.01592	0.014	0.00
004352168	5115	14.343	0.663	10.64334	4967.942159	89.58	0.18	213	0.072	0.268	1.29	0.4451	0.012	0.35
004484356	5080	14.235	0.177	1.144126	5002.774583	78.62	0.02	271	0.320	0.899	0.652	0.3817	0.025	0.00
004540632	4818	14.991	1.045	31.00996	4983.860841	89.93	0.66	98	0.030	0.315	0.826	0.2150	0.000	0.00
004579313	5363	14.811	0.008	2.112635	5002.947518	68.73	0.00	309	0.390	0.553	13.3	98.34	0.029	0.00
004633434	4902	15.362	0.233	22.27067	4967.759577	89.52	0.09	107	0.031	0.0806	1.58	0.2024	0.000	0.77
004672010	4655	14.602	0.049	0.9628780	5002.694396	41.63	0.02	271	0.904	1.97	7.26	103.9	0.038	0.00
004678171	4240	15.993	0.951	15.28859	4965.805465	89.68	0.01	111	0.045	0.474	0.996	0.4702	0.002	0.00
004737267	5156	15.145	0.471	9.523936	5001.185337	89.05	0.01	220	0.154	0.521	1.98	2.032	0.072	0.00
004757331	5092	15.725	0.087	2.362127	5001.736119	81.59	0.11	90	0.210	1.77	2.01	7.157	0.043	0.00
004758368	4594	10.805	0.044	3.750218	5003.200871	67.51	0.02	260	0.489	1.01	3.73	14.11	0.002	0.00
004773155	5447	13.592	0.733	25.70599	4989.643369	89.86	0.43	309	0.042	0.767	1.14	0.9988	0.000	0.03
004908495	4731	13.871	0.359	3.120583	4965.367280	86.08	0.01	265	0.153	0.732	1.01	0.7479	0.076	0.00
004940201	5284	14.984	0.050	8.816203	5002.550394	90.00	0.03	87	0.067	0.455	1.24	0.7023	0.000	0.93
004948863	5490	15.414	0.090	8.643652	4972.829522	87.28	0.26	89	0.070	1.33	3.05	12.37	0.001	0.00
005015913	5487	12.989	0.002	2.359939	4954.580900	72.85	0.00	277	0.312	1.06	22.9	553.2	0.004	0.00
005018787	5215	15.428	0.023	0.6071971	5002.664852	83.52	0.12	89	0.338	0.410	1.98	1.601	0.000	0.96
005036538	4199	13.349	0.758	2.122015	5001.594725	88.69	0.00	285	0.181	0.773	1.02	0.8082	0.033	0.00
005041975	5149	13.981	0.160	2.958502	5003.379626	58.09	0.00	285	0.680	0.427	2.93	3.661	0.054	0.00
005080652	5344	15.080	0.524	4.144388	5001.321781	86.69	0.01	91	0.165	0.556	0.839	0.3915	0.018	0.00
005193386	4797	13.998	0.397	21.37192	4980.205957	88.85	0.01	121	0.134	0.268	3.43	3.148	0.098	0.00
005218014	4752	12.923	0.010	10.84612	4971.331816	88.91	0.24	157	0.068	0.944	1.16	1.266	0.002	0.98
005266937	5483	14.352	0.987	5.916942	5001.400391	88.40	0.05	268	0.429	0.113	0.721	0.05881	0.020	0.00
005286786	4946	15.456	0.006	9.949612	4976.748845	88.88	0.05	230	0.049	0.817	2.81	6.433	0.002	0.98
005294739	5068	13.930	0.994	3.736174	5001.678732	76.49	0.02	278	0.555	0.138	1.85	0.4705	0.068	0.00
005300878	4631	14.767	0.823	1.279424	5002.597321	89.49	0.01	93	0.294	0.817	1.02	0.8576	0.047	0.00
005347784	5392	13.094	0.155	9.584026	5000.621695	85.60	0.01	148	0.121	1.05	1.34	1.885	0.007	0.00
005467126	4683	12.367	0.014	2.845694	5001.431451	77.08	0.15	85	0.575	0.243	1.69	0.6920	0.000	0.98
005597970	5179	12.778	0.218	6.717435	4970.209216	86.01	0.28	270	0.106	0.0127	2.74	0.09511	0.002	0.00
005598639	4847	10.201	0.135	1.297549	5003.022903	83.12	0.00	280	0.441	0.995	0.990	0.9752	0.003	0.69
005696909	5451	14.984	0.006	0.6430210	4964.688376	63.09	0.00	261	0.490	0.965	15.0	218.3	0.035	0.00
005731312	4658	13.811	0.388	7.946392	4968.092030	88.99	0.43	15	0.058	0.113	0.592	0.03952	0.000	0.20
005781192	5372	12.989	0.301	9.459957	4999.722660	88.15	0.07	295	0.077	0.518	0.645	0.2154	0.006	0.00
005802285	4791	15.349	0.017	2.417017	5003.656318	77.87	0.00	89	0.232	0.740	3.74	10.36	0.002	0.00
005802470	5418	13.764	0.337	3.791871	5001.260474	85.11	0.03	90	0.149	0.344	0.985	0.3337	0.013	0.00
005871918	4021	15.701	0.319	12.64175	4972.761250	90.00	0.16	180	0.058	0.246	1.29	0.4091	0.056	0.64
006029130	5160	14.832	0.421	12.59140	5005.516830	88.72	0.02	49	0.063	0.851	1.02	0.8859	0.002	0.00
006042116	4771	11.300	0.089	5.407156	5002.038929	80.98	0.11	54	0.211	1.60	1.32	2.789	0.004	0.00
006044064	5095	15.001	1.653	5.063280	5002.149463	83.72	0.03	75	0.389	0.145	1.78	0.4606	0.078	0.00
006060580	5308	13.460	0.019	2.313334	5003.212901	75.37	0.00	27	0.289	0.304	0.298	0.02701	0.001	0.00
006131659	4870	12.534	0.475	17.52783	4960.041441	89.37	0.02	270	0.044	0.316	0.593	0.1111	0.000	0.00
006187893	5103	11.702	0.077	0.7891775	5006.959004	64.02	0.01	274	0.634	0.135	0.349	0.01646	0.008	0.00
006191574	4208	14.353	0.233	0.000000	-50000.000000	0.00	0.00	0	0.000	0.00	0.00	0.000	0.000	0.00
006197038	4937	13.531	0.798	9.752156	5000.794386	80.21	0.19	90	0.277	0.261	2.62	1.790	0.308	0.00
006205460	5242	12.746	0.796	3.722771	5001.134908	85.88	0.01	36	0.419	0.159	2.79	1.238	0.069	0.00
006307537	4253	11.753	0.193	29.74440	4960.659149	87.35	0.04	277	0.108	0.246	4.69	5.396	0.003	0.00
006312534	4897	15.583	0.024	3.015501	5002.128021	81.73	0.36	90	0.213	16.0	2.01	64.38	0.158	0.00

Table 2 — *Continued*

Kepler ID	$T_{\rm eff}$ (K)	$m_{\rm kep}$	$\Delta m_{\rm kep}$	Period (Days)	T_0 (BJD-2450000)	i (°)	e^1	ω^1 (°)	$r_{\rm sum}$	J	k	L_r	L_1 Sine Amplitude	L_3
006359798	5452	12.932	0.071	14.15394	4959.543146	89.54	0.41	183	0.048	0.377	1.35	0.6877	0.000	0.90
006367628	5185	13.035	0.548	3.780139	5002.708087	76.36	0.02	267	0.550	0.213	0.840	0.1500	0.016	0.00
006449552	5357	14.904	0.946	20.14888	4968.810574	89.40	0.27	247	0.045	0.188	1.08	0.2176	0.001	0.00
006464285	5061	13.826	0.444	0.8436324	5003.755443	73.04	0.01	286	0.469	0.188	2.74	1.411	0.019	0.00
006466939	4920	14.454	0.733	2.285920	5003.760706	88.72	0.00	95	0.199	0.762	1.14	0.9858	0.021	0.00
006548447	5031	12.880	0.165	10.76541	5009.086049	89.90	0.11	184	0.158	0.617	3.29	6.693	0.004	0.00
006591789	5410	15.353	0.614	5.088435	5002.974423	88.48	0.01	171	0.128	0.318	0.664	0.1399	0.005	0.00
006620003	3955	15.686	0.037	3.428469	4997.172065	82.97	0.01	269	0.146	0.775	1.04	0.8436	0.000	0.00
006629332	5452	13.997	0.073	4.310363	5007.525591	84.14	0.05	90	0.122	2.95	1.46	6.279	0.130	0.00
006694186	5247	12.376	0.189	5.554204	5001.487264	80.66	0.29	271	0.223	0.00832	31.3	8.173	0.000	0.00
006697716	4898	14.424	0.279	1.443221	5008.877209	82.57	0.00	30	0.261	0.505	0.634	0.2030	0.018	0.00
006706287	5182	13.620	0.607	2.535431	5004.418517	87.19	0.00	260	0.196	0.697	0.905	0.5714	0.025	0.00
006778050	5091	14.514	0.420	0.9458108	4964.620719	81.63	0.01	276	0.389	0.822	0.855	0.6013	0.025	0.00
006841577	5478	14.875	0.270	15.53753	4973.272586	89.35	0.19	128	0.059	0.0828	1.72	0.2455	0.000	0.74
006863840	5024	15.138	0.668	3.852650	4964.746207	88.78	0.00	81	0.142	0.830	1.05	0.9234	0.060	0.00
006939670	5436	14.858	0.152	4.238755	4968.201178	79.83	0.05	91	0.235	0.889	2.80	6.980	0.145	0.00
007049486	5498	13.144	0.088	26.71855	4971.051326	88.56	0.29	21	0.052	0.684	0.498	0.1696	0.004	0.64
007097571	5266	11.267	0.153	2.213962	5005.416674	80.18	0.03	91	0.385	0.217	0.314	0.02135	0.001	0.00
007119757	5072	15.608	0.249	0.7429393	4980.909123	71.04	0.02	86	0.541	1.10	1.58	2.750	0.058	0.00
007125636	4358	15.507	0.266	6.490765	4978.048116	87.67	0.02	214	0.081	0.835	0.929	0.7198	0.005	0.00
007128918	5386	15.758	0.142	7.118892	4984.394210	88.47	0.01	54	0.085	0.573	0.885	0.4486	0.004	0.70
007129465	5182	15.316	0.427	5.491840	4966.171031	87.83	0.00	271	0.107	0.856	0.941	0.7591	0.004	0.00
007200102	5207	15.213	0.538	14.66695	4972.573070	88.65	0.42	124	0.054	0.564	0.751	0.3181	0.000	0.04
007220322	4887	11.884	0.009	0.7521433	5002.397213	53.82	0.01	85	0.657	1.55	11.1	190.1	0.130	0.00
007257373	5311	13.424	0.745	10.46686	4955.658505	89.72	0.00	89	0.113	1.02	0.922	0.8700	0.001	0.00
007284688	4191	11.234	0.088	0.6461003	5002.783432	64.97	0.00	124	0.552	1.22	2.29	6.374	0.055	0.00
007624297	5135	14.928	0.222	18.01846	4981.666593	88.97	0.05	76	0.042	0.0661	1.73	0.1989	0.000	0.74
007670617	4876	15.517	0.450	24.70190	4969.146845	89.85	0.28	308	0.033	0.201	0.711	0.1018	0.000	0.35
007671594	3717	15.815	0.165	1.410329	4965.398972	84.54	0.00	302	0.138	0.612	1.19	0.8632	0.039	0.00
007691527	5354	15.431	0.463	4.800056	5002.382912	87.47	0.10	130	0.115	1.07	1.21	1.573	0.073	0.00
007749318	5211	14.528	0.341	2.371784	5003.689256	80.47	0.18	270	0.246	0.0569	3.32	0.6277	0.078	0.00
007769072	4858	13.886	0.003	0.6088726	5002.799849	57.25	0.00	72	0.583	1.18	21.8	559.9	0.016	0.00
007798259	4619	15.726	0.411	1.734306	5005.720952	84.29	0.03	270	0.200	0.310	1.22	0.4600	0.070	0.00
007830321	5347	15.476	0.008	2.027248	5003.200747	73.45	0.00	242	0.301	0.672	6.41	27.63	0.010	0.00
007842610	5375	15.289	0.021	1.943760	5001.841852	76.41	0.00	270	0.271	1.32	4.25	23.80	0.027	0.00
007846730	5476	12.956	0.381	11.02825	4969.966521	88.40	0.02	151	0.101	0.599	1.88	2.126	0.000	0.12
007885570	5398	11.679	0.223	1.729021	5001.851398	74.44	0.05	85	0.454	0.747	3.41	8.661	0.237	0.00
007947631	4823	15.179	0.022	2.516590	4987.092316	79.51	0.01	89	0.209	1.13	3.03	10.33	0.008	0.00
007955301	4821	12.672	0.007	15.30817	4960.464666	86.04	0.01	174	0.078	1.42	8.19	95.41	0.001	0.00
007987749	5349	14.461	0.095	17.03109	4978.541107	88.17	0.14	187	0.046	0.398	0.495	0.09742	0.000	0.00
008075618	5288	15.674	0.119	17.56154	4970.923092	88.76	0.02	90	0.031	1.11	0.961	1.027	0.000	0.00
008075755	4075	13.407	0.009	0.4962355	4964.752415	66.36	0.01	94	0.471	0.516	0.0939	0.004556	0.000	0.00
008076905	4214	15.613	0.011	0.4180906	5003.192377	51.07	0.01	279	0.715	1.67	11.8	231.1	0.083	0.00
008094140	4200	15.159	0.606	0.7064196	4973.624150	86.37	0.01	265	0.326	0.274	0.628	0.1079	0.038	0.00
008095110	5370	13.171	0.036	4.206510	4974.280246	76.85	0.02	91	0.300	1.56	4.03	25.26	0.035	0.00
008097825	5329	13.283	0.261	2.937050	4966.633044	78.40	0.00	286	0.343	0.645	1.50	1.449	0.028	0.00
008143170	4957	12.850	0.058	28.78627	4970.110463	85.83	0.20	255	0.103	0.269	6.55	11.55	0.001	0.00
008145789	4829	15.314	0.027	1.670636	5000.039740	75.30	0.01	272	0.311	0.917	5.66	29.34	0.016	0.00
008181016	5179	14.677	0.008	0.7090293	4965.187959	75.06	0.20	270	0.434	0.197	1.37	0.3690	0.000	0.98
008210721	5412	14.274	0.080	22.67256	4971.153407	87.76	0.29	64	0.057	0.234	3.46	2.809	0.000	0.75
008231877	4956	14.932	0.024	2.615519	4975.237630	83.45	0.15	90	0.162	1.87	0.511	0.4880	0.000	0.79
008279765	5464	15.235	0.051	2.757746	4965.474866	83.85	0.01	282	0.169	0.0539	0.208	0.002322	0.003	0.00
008288719	5090	13.276	0.043	1.510074	4972.744897	75.00	0.01	95	0.312	1.04	2.58	6.916	0.007	0.00
008296467	5316	15.177	0.987	10.30327	4970.167785	89.99	0.26	320	0.069	0.623	1.06	0.7061	0.006	0.00
008358008	5020	14.674	0.012	10.06506	4968.250048	89.42	0.06	79	0.054	0.533	1.51	1.216	0.000	0.98
008364119	5443	12.408	0.462	7.735857	4970.986699	88.29	0.03	44	0.093	0.897	0.849	0.6471	0.003	0.00
008379547	4861	13.373	0.174	6.041994	4959.163251	81.83	0.35	270	0.222	0.0668	7.25	3.510	0.083	0.00
008397675	5462	13.501	0.002	0.5532564	5001.856348	83.35	0.16	91	0.230	0.933	2.95	8.128	0.092	0.99
008411947	5086	15.300	0.860	1.797734	5003.785574	88.27	0.02	96	0.265	0.607	1.12	0.7612	0.050	0.00
008444552	5388	13.643	0.083	1.178041	4964.597354	77.49	0.11	90	0.323	2.28	1.96	8.734	0.021	0.00
008453324	4733	11.516	0.010	2.524694	5001.646619	72.45	0.00	82	0.341	1.42	5.66	45.59	0.016	0.00
008543278	4950	14.608	0.073	7.549631	4998.208506	88.40	0.12	276	0.052	0.187	0.451	0.03811	0.000	0.57
008559863	5154	12.723	0.055	22.46892	4953.814854	88.21	0.04	217	0.054	0.720	0.437	0.1377	0.002	0.56
008574270	5061	15.166	0.031	15.11963	4972.699012	87.27	0.29	321	0.059	0.0360	0.955	0.03285	0.000	0.00
008580438	5307	14.502	0.152	6.495852	5000.947823	90.00	0.01	80	0.108	0.0314	0.315	0.003107	0.004	0.00
008581232	4314	15.381	0.037	4.012679	5003.764787	87.32	0.33	133	0.086	0.279	0.138	0.005326	0.000	0.00
008616873	5486	15.237	0.015	0.5760785	5002.245893	81.58	0.14	86	0.437	0.140	2.17	0.6544	0.089	0.98
008655458	5210	14.585	0.008	1.594193	5002.299400	88.86	0.03	78	0.397	0.183	0.472	0.04073	0.000	0.98
008718273	4577	10.565	0.006	6.958070	4997.699036	89.55	0.03	269	0.050	0.740	0.0474	0.001664	0.000	0.00
008719897	4905	12.392	0.262	3.151596	4955.232895	80.22	0.02	90	0.315	1.02	1.13	1.291	0.015	0.00
008841616	4550	12.833	0.133	1.679564	4966.238497	61.97	0.02	71	0.650	0.0436	0.639	0.01781	0.022	0.00
008846978	5191	13.371	0.225	1.379281	4970.036969	64.68	0.06	312	0.556	0.0263	3.72	0.3635	0.196	0.58
008848104	5447	12.372	0.041	0.8248496	4972.049484	61.47	0.01	100	0.538	0.307	6.94	14.79	0.029	0.00
008906676	5249	12.121	0.167	8.209521	4967.062429	88.28	0.03	89	0.075	0.118	1.71	0.3441	0.000	0.78
008971432	5057	15.487	0.063	0.6243809	5001.634891	65.63	0.03	89	0.533	0.0555	0.299	0.004965	0.001	0.00

Table 2 — *Continued*

Kepler ID	T_{eff} (K)	m_{kep}	Δm_{kep}	Period (Days)	T_0 (BJD-2450000)	i (°)	e^1	ω^1 (°)	r_{sum}	J	k	L_r	L_1 Sine Amplitude	L_3
009001468	4949	15.200	0.339	17.32833	4975.727756	89.41	0.52	239	0.043	0.216	1.54	0.5119	0.000	0.57
009029486	5368	13.630	0.342	6.277180	4965.329729	89.54	0.00	279	0.094	0.903	0.981	0.8686	0.007	0.45
009098810	5126	13.448	0.443	8.258238	4972.758295	88.41	0.16	87	0.079	0.957	0.832	0.6620	0.006	0.00
009210828	4893	13.221	0.205	1.656351	4977.002807	80.24	0.02	90	0.269	0.756	1.16	1.016	0.004	0.00
009266285	4184	14.072	0.072	5.613843	4965.571978	82.83	0.27	91	0.182	3.49	1.65	9.496	0.014	0.00
009284741	5085	14.807	0.516	20.72910	4974.226975	89.42	0.37	42	0.041	1.15	1.05	1.265	0.006	0.00
009291629	4629	13.957	0.168	20.69085	4966.893246	84.62	0.13	271	0.214	0.346	4.57	7.243	0.151	0.00
009328852	4338	15.330	0.550	0.6458239	5008.159243	84.39	0.04	82	0.410	0.0705	0.519	0.01901	0.047	0.00
009334490	5105	15.695	0.017	18.84520	4982.944981	89.46	0.02	129	0.038	0.797	0.547	0.2389	0.000	0.96
009346655	4183	14.299	0.144	0.8716196	4965.119502	81.56	0.50	90	0.262	6.12	1.50	13.73	0.380	0.00
009412462	5350	14.846	0.518	10.18653	4965.527836	87.39	0.03	230	0.143	0.747	1.19	1.065	0.016	0.00
009418994	5053	13.396	0.021	32.00590	4969.494447	89.65	0.23	54	0.024	0.136	0.668	0.06079	0.000	0.96
009474485	4469	14.884	0.668	1.025164	4965.292428	87.18	0.00	5	0.329	0.864	1.02	0.9024	0.033	0.00
009574614	5276	15.933	0.011	1.964342	5002.018849	78.41	0.01	238	0.220	1.01	4.37	19.23	0.001	0.00
009597095	5331	15.945	0.073	2.745608	5003.145923	81.81	0.02	269	0.203	0.121	0.377	0.01723	0.001	0.00
009632895	5425	13.552	0.097	27.32202	4965.424356	87.89	0.03	257	0.046	0.0428	11.9	6.042	0.000	0.46
009639265	5004	15.575	0.370	0.5063492	4964.814722	75.19	0.02	275	0.520	0.888	0.765	0.5194	0.068	0.00
009658832	4545	13.638	0.029	0.4568510	5002.649683	56.54	0.01	80	0.683	0.335	0.163	0.008909	0.002	0.00
009665503	5141	15.217	0.656	11.56806	4970.339984	89.46	0.28	330	0.063	0.383	0.694	0.1844	0.000	0.00
009714358	4825	14.998	0.283	6.479757	4999.785837	86.63	0.26	272	0.089	0.0295	3.94	0.4572	0.000	0.13
009761199	4060	15.692	0.014	1.383998	4964.727100	74.47	0.00	128	0.289	1.14	3.00	10.29	0.009	0.00
009762519	5435	13.711	0.152	7.515083	4971.079973	86.05	0.18	282	0.095	0.0521	2.31	0.2778	0.007	0.00
009837578	5359	15.726	0.698	20.73369	4965.845828	89.44	0.16	87	0.048	0.681	1.26	1.083	0.000	0.00
009851126	4164	13.183	0.097	8.480306	4968.853813	89.89	0.21	18	0.129	0.137	0.257	0.009052	0.000	0.03
009912977	5158	13.726	0.442	1.887885	5002.578442	79.82	0.01	91	0.473	1.01	1.17	1.380	0.002	0.00
009913798	4659	14.945	0.218	2.143443	5002.935126	83.44	0.01	271	0.269	0.173	0.409	0.02886	0.001	0.00
009934208	4258	15.507	0.166	9.058852	4970.337139	85.96	0.14	51	0.091	0.193	5.49	5.819	0.002	0.00
009944201	4737	15.069	0.032	0.7215318	5002.227862	86.33	0.07	90	0.307	0.215	1.71	0.6296	0.091	0.96
009944421	5304	15.137	0.349	7.095304	4968.370748	86.24	0.26	69	0.100	0.637	1.18	0.8853	0.024	0.00
010014830	4324	14.827	0.897	3.030715	5003.492462	85.95	0.00	185	0.549	0.279	1.80	0.9018	0.058	0.00
010026457	5222	15.390	0.089	9.934463	5005.612121	89.71	0.13	320	0.109	0.990	0.970	0.9321	0.000	0.84
010090246	5442	13.567	0.171	2.285607	5003.110556	56.54	0.03	89	0.695	0.560	2.32	3.022	0.038	0.00
010095484	5486	14.382	0.008	0.6777383	5002.579926	29.31	0.01	97	0.906	0.536	16.2	140.0	0.060	0.00
010129482	4558	15.994	0.268	0.8462873	5002.429877	80.44	0.00	76	0.326	0.190	0.615	0.07199	0.011	0.00
010189523	5002	15.856	0.117	1.013960	5002.929802	74.89	0.05	89	0.325	1.29	0.530	0.3627	0.039	0.00
010215422	5427	14.608	0.444	24.39590	4987.127475	89.06	0.29	9	0.045	0.207	1.43	0.4202	0.000	0.44
010264202	5207	15.777	0.144	1.035161	5002.815429	75.46	0.01	272	0.373	0.672	0.955	0.6130	0.004	0.00
010292465	5258	14.956	0.152	1.353325	5002.832143	73.64	0.00	0	0.348	0.0940	4.64	2.023	0.068	0.34
010330495	5132	14.724	0.075	18.06030	4971.608312	85.34	0.14	254	0.117	0.150	10.5	16.46	0.003	0.00
010346522	5286	14.404	1.204	3.988565	5001.472319	85.90	0.01	63	0.585	0.188	0.814	0.1246	0.008	0.00
010491544	4835	13.436	0.031	22.77214	4973.487861	86.42	0.54	56	0.089	15.6	1.34	27.91	0.017	0.00
010592163	5482	15.095	0.098	14.76289	4966.772333	88.98	0.32	329	0.057	0.486	0.628	0.1916	0.000	0.73
010613718	5080	12.735	0.010	1.175802	4966.821353	74.39	0.01	269	0.307	0.966	8.52	70.13	0.006	0.00
010711646	4339	15.787	0.204	0.7376206	4997.149560	78.07	0.08	270	0.343	0.134	1.16	0.1808	0.046	0.42
010753734	5446	13.564	0.725	19.40624	4982.807297	89.74	0.52	18	0.051	0.823	0.849	0.5942	0.005	0.00
010794242	5459	14.170	0.269	7.143779	4970.803174	89.19	0.08	247	0.102	0.0887	0.425	0.01604	0.010	0.00
010794405	5479	14.713	0.005	0.9522659	4979.620590	40.08	0.00	237	0.821	3.37	12.9	557.6	0.192	0.00
010809677	4995	13.942	0.008	7.042849	4970.731749	80.78	0.00	271	0.172	0.968	3.55	12.20	0.000	0.00
010936427	5082	14.419	0.756	14.35935	4971.843223	88.64	0.02	84	0.116	0.401	1.72	1.192	0.042	0.00
010979716	3932	15.774	0.125	10.68394	4967.091349	88.05	0.15	278	0.054	0.307	0.718	0.1586	0.006	0.00
010991989	5021	10.282	0.012	0.9744771	4965.368901	85.97	0.09	268	0.358	0.568	0.597	0.2028	0.000	0.97
010992733	5274	15.124	0.728	18.52628	4977.193722	89.99	0.38	26	0.055	0.704	0.777	0.4255	0.006	0.00
011124509	5417	14.735	0.018	8.893240	4968.729831	85.98	0.01	269	0.080	0.393	1.34	0.7016	0.001	0.74
011134079	5201	14.864	0.232	1.260506	4965.061893	73.28	0.01	265	0.368	0.134	4.48	2.688	0.043	0.00
011147460	4855	13.912	0.009	4.107429	4965.943730	73.69	0.00	71	0.316	0.548	0.139	0.01052	0.000	0.00
011232745	5204	15.973	0.056	9.633799	4970.918869	89.91	0.03	90	0.037	0.574	1.67	1.609	0.058	0.91
011233911	5193	14.742	0.285	4.959761	4969.120822	85.16	0.01	90	0.171	0.789	2.19	3.776	0.103	0.00
011235323	5071	13.486	0.496	19.67035	4965.522562	89.28	0.06	270	0.137	0.458	0.598	0.1636	0.006	0.00
011287726	5167	14.176	0.159	4.736985	4970.064587	78.94	0.07	271	0.258	0.175	1.53	0.4081	0.005	0.00
011350389	5124	15.724	0.037	1.512708	4969.562269	83.00	0.05	270	0.172	0.213	8.74	16.24	0.019	0.59
011391181	5218	15.257	0.276	8.617414	4972.068740	87.23	0.20	30	0.081	0.923	1.15	1.228	0.024	0.00
011391667	5394	12.923	0.011	1.083646	4954.131479	74.63	0.00	292	0.320	0.497	0.116	0.006724	0.000	0.00
011455795	4477	15.414	0.072	1.057351	4964.791193	81.87	0.00	0	0.221	0.0229	7.44	1.271	0.108	0.90
011546211	3682	15.155	0.083	2.194447	4966.712688	85.75	0.67	90	0.133	88.2	0.454	18.17	0.756	0.00
011671660	4867	13.350	0.089	8.702917	4956.587112	72.47	0.03	271	0.368	0.718	5.29	20.08	0.233	0.00
011768970	5038	12.658	0.012	15.54223	4959.412961	87.15	0.87	82	0.089	28.7	1.42	57.58	0.000	0.42
011858541	5375	14.215	0.045	5.674410	4968.755298	81.16	0.06	355	0.180	0.421	4.60	8.922	0.006	0.00
011968514	4940	11.449	0.005	2.073289	5002.408007	73.94	0.01	259	0.304	1.32	16.0	338.4	0.037	0.00
011975363	5482	15.409	0.578	3.518364	4967.411791	88.02	0.01	89	0.180	0.916	1.08	1.061	0.018	0.00
012004679	5432	13.231	0.833	5.042429	4955.770424	89.85	0.01	77	0.115	0.803	0.997	0.7988	0.008	0.00
012004834	3576	14.718	0.333	0.2623169	4964.398367	72.47	0.06	269	0.517	1.04	1.56	2.532	0.018	0.00
012105785	5349	13.032	0.021	31.95107	4975.706638	87.34	0.18	114	0.056	2.81	0.507	0.7219	0.000	0.66
012351927	4641	15.520	0.086	10.11594	4972.982326	85.41	0.01	119	0.087	0.0699	7.19	3.613	0.000	0.00
012356914	5368	15.529	0.621	27.30710	4976.502419	89.94	0.44	74	0.035	0.157	0.636	0.06344	0.001	0.00
012365000	5080	13.573	0.028	1.262660	4986.658328	77.85	0.11	269	0.283	0.148	0.912	0.1230	0.025	0.70

Table 2 — *Continued*

Kepler ID	T_{eff} (K)	m_{kep}	Δm_{kep}	Period (Days)	T_0 (BJD-2450000)	i (°)	e[1]	ω[1] (°)	r_{sum}	J	k	L_r	L_1 Sine Amplitude	L_3
012367017	5004	14.730	0.008	1.222133	4970.925867	59.96	0.00	290	0.540	0.806	18.6	277.5	0.026	0.00
012367310	4965	13.835	0.044	8.627137	4972.995164	81.33	0.02	314	0.167	0.147	5.54	4.518	0.017	0.00
012400729	4949	15.227	0.149	0.9317268	4965.479857	72.86	0.13	196	0.366	0.000549	8.92	0.04368	0.219	0.88
012418816	4583	12.402	0.581	1.521896	4965.395396	87.12	0.01	88	0.248	1.00	1.04	1.082	0.038	0.00
012470530	4725	15.300	0.658	8.207057	4968.824442	88.44	0.38	347	0.072	0.302	0.979	0.2889	0.000	0.03
012557713	4594	14.853	0.068	7.214603	4965.498124	87.06	0.43	92	0.077	12.6	0.412	2.134	0.000	0.17
012599700	3887	15.784	0.120	1.017821	4968.317001	87.78	0.03	268	0.136	0.433	1.24	0.6686	0.363	0.87
012645761	4844	13.368	0.018	5.419663	4958.954807	81.82	0.34	90	0.212	23.8	1.91	86.59	0.185	0.00

---

[1] Although the values for e and ω are presented in this table for ease of reading, the values of $e \cdot \cos(\omega)$ and $e \cdot \sin(\omega)$ were actually solved for in the analysis.

Table 3
Temperature, Mass, and Radius Estimates for the 95 New LMMS DDEB Candidates with Amplitudes ≥ 0.1 Magnitudes and Both Masses < 1.0 $M_\odot$

Kepler ID	Period (Days)	$T_{\rm eff}$(K)	T_1(K)	T_2(K)	M_1($M_\odot$)	M_2($M_\odot$)	R_1($R_\odot$)	R_2($R_\odot$)
002162994	4.102	5410	5593	5038	0.96	0.86	1.39	1.24
002437452	14.47	5398	5591	4647	0.96	0.79	1.40	1.13
002719873	17.28	5086	5246	4382	0.90	0.73	1.08	0.86
002852560	11.96	5381	5385	5378	0.93	0.92	1.06	1.06
003003991	7.245	5366	5554	4598	0.96	0.78	0.83	0.67
003102024	13.78	5117	5160	5069	0.89	0.87	0.79	0.78
003241344	3.913	5422	5461	3688	0.94	0.52	0.94	0.49
003241619	1.703	5165	5344	4622	0.92	0.79	1.04	0.88
003458919	0.8920	5063	5206	4254	0.89	0.70	1.08	0.83
003730067	0.2941	4099	4158	4010	0.68	0.64	0.62	0.58
003848919	1.047	5226	5238	5214	0.90	0.90	1.10	1.10
004049124	4.804	5349	5501	4347	0.95	0.73	1.30	0.97
004077442	0.6929	4523	4643	4094	0.79	0.66	1.03	0.84
004346875	4.694	5339	5367	3599	0.92	0.46	1.21	0.56
004352168	10.64	5115	5281	4744	0.91	0.81	0.93	0.82
004484356	1.144	5080	5250	4636	0.90	0.79	0.94	0.81
004540632	31.01	4818	4953	4190	0.85	0.69	0.80	0.63
004633434	22.27	4902	5041	4219	0.86	0.69	0.67	0.52
004678171	15.29	4240	4331	4048	0.72	0.65	0.68	0.60
004773155	25.71	5447	5448	5447	0.94	0.94	0.96	0.96
004908495	3.121	4731	4791	4655	0.82	0.79	0.82	0.79
005036538	2.122	4199	4236	4155	0.70	0.68	0.71	0.69
005080652	4.144	5344	5536	4858	0.95	0.83	1.17	1.01
005300878	1.279	4631	4667	4590	0.80	0.78	0.87	0.85
005597970	6.717	5179	5284	4060	0.91	0.65	1.08	0.74
005731312	7.946	4658	4701	3583	0.80	0.45	0.68	0.36
005781192	9.460	5372	5546	4482	0.95	0.76	0.97	0.75
005802470	3.792	5418	5620	4859	0.97	0.83	1.00	0.86
005871918	12.64	4021	4052	3983	0.65	0.63	0.79	0.76
006029130	12.59	5160	5201	5114	0.89	0.88	0.88	0.86
006131659	17.53	4870	4970	3972	0.85	0.63	0.84	0.59
006449552	20.15	5357	5537	4532	0.95	0.77	0.93	0.74
006464285	0.8436	5061	5159	4923	0.89	0.84	1.09	1.03
006466939	2.286	4920	4925	4916	0.84	0.84	0.87	0.86
006591789	5.088	5410	5560	4342	0.96	0.73	1.09	0.81
006697716	1.443	4898	5036	4215	0.86	0.69	0.91	0.71
006706287	2.535	5182	5327	4931	0.91	0.85	0.96	0.89
006778050	0.9458	5091	5223	4872	0.90	0.83	0.98	0.91
006841577	15.54	5478	5676	4676	0.98	0.80	1.03	0.83
006863840	3.853	5024	5050	4997	0.87	0.86	0.88	0.87
007119757	0.7429	5072	5242	4607	0.90	0.78	1.20	1.03
007125636	6.491	4358	4417	4277	0.74	0.71	0.69	0.66
007128918	7.119	5386	5574	4968	0.96	0.85	0.86	0.76
007129465	5.492	5182	5269	5069	0.90	0.87	0.87	0.83
007200102	14.67	5207	5390	4643	0.93	0.79	0.88	0.74
007624297	18.02	5135	5291	4352	0.91	0.73	0.81	0.63
007670617	24.70	4876	4971	3945	0.85	0.62	0.80	0.56
007671594	1.410	3717	3773	3597	0.56	0.46	0.40	0.32
007691527	4.800	5354	5492	5138	0.94	0.88	0.87	0.81
007749318	2.372	5211	5347	4991	0.92	0.86	1.16	1.07
007798259	1.734	4619	4735	4386	0.81	0.74	0.74	0.67
007846730	11.03	5476	5667	5079	0.98	0.87	1.37	1.22
008075618	17.56	5288	5301	5275	0.91	0.91	0.55	0.54
008094140	0.7064	4200	4266	3598	0.71	0.46	0.70	0.44
008296467	10.30	5316	5427	5159	0.93	0.89	0.86	0.82
008364119	7.736	5443	5581	5232	0.96	0.90	0.97	0.91
008411947	1.798	5086	5168	4980	0.89	0.85	1.01	0.97
008580438	6.496	5307	5314	3348	0.91	0.23	1.31	0.35
008906676	8.210	5249	5436	4709	0.93	0.80	0.84	0.71
009001468	17.33	4949	5089	4676	0.87	0.80	0.76	0.69
009029486	6.277	5368	5421	5309	0.93	0.91	0.83	0.81
009098810	8.258	5126	5240	4956	0.90	0.85	0.84	0.79
009210828	1.656	4893	4898	4888	0.84	0.84	0.94	0.94
009284741	20.73	5085	5156	4998	0.88	0.86	0.80	0.78
009328852	0.6458	4338	4357	3375	0.73	0.25	0.94	0.34
009346655	0.8716	4183	4232	3512	0.70	0.39	0.67	0.37
009474485	1.025	4469	4492	4444	0.76	0.75	0.81	0.80
009639265	0.5063	5004	5147	4730	0.88	0.81	0.87	0.79
009665503	11.57	5141	5293	4321	0.91	0.72	0.90	0.69
009714358	6.480	4825	4964	4522	0.85	0.77	0.81	0.72
009762519	7.515	5435	5528	4050	0.95	0.65	0.95	0.62
009837578	20.73	5359	5390	5327	0.93	0.91	0.95	0.94
009934208	9.059	4258	4347	3743	0.73	0.55	1.04	0.76
009944421	7.095	5304	5348	5255	0.92	0.90	0.96	0.94

Table 3 — *Continued*

Kepler ID	Period (Days)	T_{eff}(K)	T_1(K)	T_2(K)	M_1($M_\odot$)	M_2($M_\odot$)	R_1($R_\odot$)	R_2($R_\odot$)
010129482	0.8463	4558	4622	3669	0.79	0.51	0.83	0.51
010189523	1.014	5002	5143	4239	0.88	0.70	0.91	0.70
010215422	24.40	5427	5625	4944	0.97	0.85	1.04	0.91
010264202	1.035	5207	5347	4971	0.92	0.85	1.01	0.93
010292465	1.353	5258	5417	4965	0.93	0.85	1.15	1.05
010711646	0.7376	4339	4440	3877	0.75	0.59	0.74	0.57
010753734	19.41	5446	5603	5183	0.97	0.89	0.99	0.91
010794242	7.144	5459	5490	3633	0.94	0.49	1.20	0.58
010979716	10.68	3932	3996	3530	0.63	0.41	0.68	0.43
010992733	18.53	5274	5457	4848	0.94	0.83	1.04	0.91
011134079	1.261	5201	5381	4732	0.92	0.81	1.17	1.01
011233911	4.960	5193	5370	4531	0.92	0.77	1.38	1.12
011391181	8.617	5218	5288	5133	0.91	0.88	0.88	0.85
011975363	3.518	5482	5507	5457	0.95	0.94	1.09	1.08
012004679	5.042	5432	5514	5330	0.95	0.92	0.89	0.86
012004834	0.2623	3576	3620	3468	0.48	0.34	0.48	0.35
012356914	27.31	5368	5455	4003	0.94	0.63	0.93	0.60
012400729	0.9317	4949	5005	3715	0.86	0.54	1.03	0.61
012418816	1.522	4583	4603	4563	0.78	0.77	0.81	0.80
012470530	8.207	4725	4863	4245	0.83	0.70	0.78	0.64
012599700	1.018	3887	3936	3816	0.61	0.57	0.32	0.30

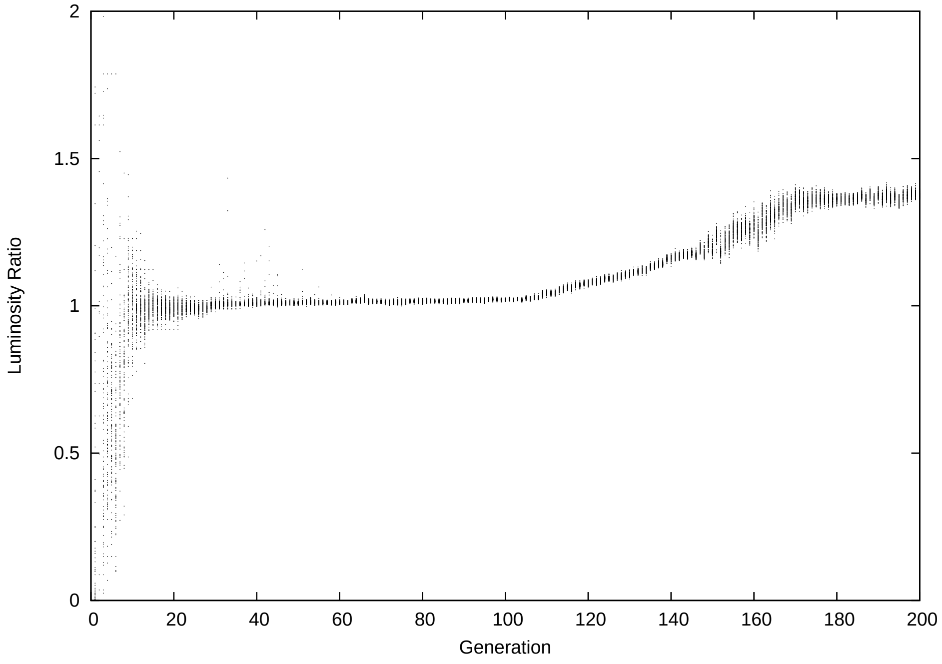
Luminosity Ratio
Generation
0
0.5
1
1.5
2
0
20
40
60
80
100
120
140
160
180
200